LBNL-42925
Preprint

ERNEST ORLANDO LAWRENCE
BERKELEY NATIONAL LABORATORY

Conceptual Model of the Geometry and Physics of Water Flow in a Fractured Basalt Vadose Zone: Box Canyon Site, Idaho

Boris Faybishenko, Christine Doughty, Michael Steiger, Jane C.S. Long, Tom Wood, Janet Jacobsen, Jason Lore, and Peter T. Zawislanski

Earth Sciences Division

March 1999

Submitted to
Water Resources Research

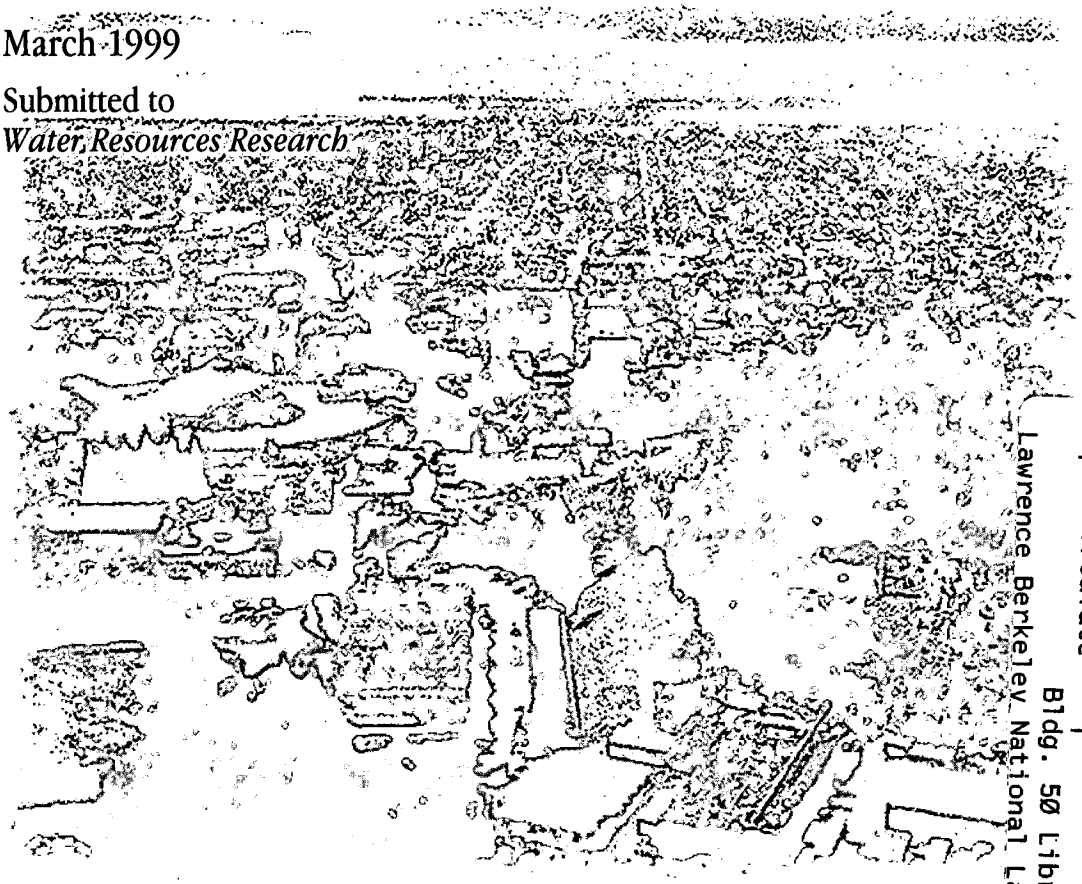

DISCLAIMER

LBNL-42925

Conceptual Model of the Geometry and Physics of Water Flow in a Fractured Basalt Vadose Zone: Box Canyon Site, Idaho

Boris Faybishenko,[1] Christine Doughty,[1] Michael Steiger,[1]
Jane C. S. Long,[2] Tom Wood,[3] Janet Jacobsen,[1] Jason Lore,[4] and
Peter T. Zawislanski[1]

[1]Earth Sciences Division
Ernest Orlando Lawrence Berkeley National Laboratory
University of California
Berkeley, California

[2]Mackay School of Mines
University of Nevada, Reno
Reno, Nevada

[3]Parsons Engineering, Inc.
Idaho Falls, ID

[4]Stanford University
Stanford, California

March 1999

This work was funded by the Office of Environmental Management, Office of Science and Technology, Characterization, Monitoring, and Sensor Technology Crosscutting Program of the U.S. Department of Energy under Contract No. DE-AC03-76SF00098.

Abstract

A conceptual model of the geometry and physics of water flow in a fractured basalt vadose zone was developed based on the results of lithological studies and a series of ponded infiltration tests conducted at the Box Canyon site near the Idaho National Engineering and Environmental Laboratory (INEEL) in Idaho. The infiltration tests included one two-week test in 1996, three two-day tests in 1997, and one four-day test in 1997. For the various tests, initial infiltration rates ranged from 4.1 cm/day to 17.7 cm/day and then decreased with time, presumably due to mechanical or microbiological clogging of fractures and vesicular basalt in the near-surface zone, as well as the effect of entrapped air. The subsurface moisture redistribution was monitored with tensiometers, neutron logging, time domain reflectrometry and ground penetrating radar. A conservative tracer, potassium bromide, was added to the pond water at a concentration of 3 g/L to monitor water flow with electrical resistivity probes and water sampling. Analysis of the data showed evidence of preferential flow rather than the propagation of a uniform wetting front. We propose a conceptual model describing the saturation-desaturation behavior of the basalt, in which rapid preferential flow through vertical column-bounding fractures occurs from the surface to the base of the basalt flow. After the rapid wetting of column-bounding fractures, a gradual wetting of other fractures and the basalt matrix occurs. Fractures that are saturated early in the tests may become desaturated thereafter, which we attribute to the redistribution of water between fractures and matrix. Lateral movement of water was also observed within a horizontal central fracture zone and rubble zone, which could have important implications for contaminant accumulation at contaminated sites.

1. Introduction

1.1. Motivation

The Department of Energy (DOE) faces the remediation of several contaminated sites with fractured basalt vadose zones, where chemical and radioactive wastes released from shallow ponds and deep wells have traveled downward sporadically through narrow fracture pathways that are difficult, if not impossible, to detect. In addition, perched water zones create a system of hydraulic baffles that are poorly understood. Thus, the behavior of contaminants at these sites has been very difficult to predict. An important issue in the remediation of these contaminated sites is the development of an appropriate conceptual model that describes the geometry of the flow domain and the physics of water flow through it.

1.2. Importance of a Conceptual Model

The development of a conceptual model (Figure 1) is an important step because an incorrect model can lead to significant errors in the development of mathematical and numerical models, thus adversely affecting predictions and planning remediation efforts. The development of a conceptual model is based on the analysis and simplification of data collected during field and laboratory experiments. In general, conceptual models that describe water flow include a description of the hydrologic components of the system, and how mass is transferred between these components.

In classic hydrogeological analysis, the system components are commonly taken to be cubes of equivalent porous medium that tessellate the volume of interest [Long et al., 1982]. The rules used to describe flow in an unsaturated medium are commonly given by Richards' equation that describes water flow as a function of the hydraulic head gradient and effective permeability (the product of intrinsic and relative permeability). However, a common problem for fractured rocks is that the medium does not behave like an equivalent continuum [Long et al., 1982]. On a given scale of observation, there may not

be a permeability tensor that can describe the relationship between flow and gradient. In this case, we may need to specify a network of conducting elements that mimic the behavior of the rock mass under arbitrary boundary conditions. The definitions of the parameters depend on both the conceptual and mathematical models of flow that are used to describe the system behavior. Without a conceptual model, we do not know what tests to conduct, what parameters to measure, where to place probes, or what probes to use. Conversely, without the data, we cannot develop a conceptual model. This situation requires an iterative approach, in which we conduct a series of tests, and concurrently, develop a conceptual model of water flow to refine our tests.

The development of a conceptual model for water flow in a fractured rock vadose zone is particularly difficult for three reasons:

1. The contrasts in permeability of the basalt fractures and matrix may be extreme and localized. Fractures with permeability as high as 30 m/day [Wood and Norrell, 1996], or even higher [Heath, 1984], are imbedded in a rock matrix with permeability as low as 10^{-8} m/day.

2. Water flow in a fracture network depends strongly on the interconnection or connectivity of the fractures when the matrix permeability is much less than the fracture permeability [Long, 1996]. In a given system, many, or in some cases nearly all observable fractures may be non-conductive and play no significant role in flow, even when they appear to be inter-connected [Knutson et al., 1993; Priest, 1993]. Fractures may be non-conductive because apertures are closed under the ambient stress state or by mineral precipitation. Fracture conductivity may decrease during an infiltration event due to clogging, sealing, or air entrapment.

3. The design of borehole tests and interpretation of data in fractured rocks are complicated because the response in a monitoring well may only be from a single fracture [Long, 1996]. In this case, measuring the test response is equivalent to measuring the response in a single pore in a porous medium. Therefore, "point"

measurements in a fractured system cannot reveal processes that result from the interaction of features at many different scales that are related to each other in a complex manner.

1.3. Purpose and Structure

The purpose of this paper is to discuss the development of a conceptual model of the geometry of the flow domain and the physics of water flow in a fractured basalt vadose zone based on results from a detailed site characterization and a series of ponded infiltration tests using a tracer. The field experiments were conducted at the Box Canyon site, located in the Eastern Snake River Plain near the INEEL (Figure 2). The area called Box Canyon is adjacent to the Big Lost River, which is a tributary to the Snake River. The Box Canyon site is an environmentally clean analog site for contaminated sites at the INEEL. Minimal soil cover and a nearby cliff-face exposure provide an excellent opportunity to study the relationships between the fracture pattern and the hydrogeologic response to the infiltration tests.

Background information gathered during earlier studies at the INEEL, most notably the Large Scale Infiltration Test (LSIT), is reviewed before the discussion of the Box Canyon infiltration tests. Then, the lithology and fracture pattern at the Box Canyon site are described and the conceptual model of the fracture pattern is presented. The main section of the paper focuses on the description of the tests and a discussion of the characteristics of water flow during the tests. Some results and insights from a numerical modeling study are also included.

2. The Snake River Plain Lithology and Review of the Large Scale Infiltration Test

The Snake River Plain is primarily composed of fractured Quaternary basalt flow units, inter-layered with sedimentary deposits [Welhan and Reed, 1997]. Sedimentary inter-beds may separate basalt flow units that were formed at widely separated times, and their

thickness may range from a few centimeters to as much as 15 m. Some have great areal extent, while others are of limited extent. Basalt flow units are comprised of a number of basalt flows arising from the same eruption event. Individual basalt flows, 3 m to 12 m thick, are typically highly fractured at the flow margins, of limited areal extent, and have a lobate geometry in plan view. The basalt flows show an extreme elongation in one direction, giving them a finger or lenticular structure with a width typically ranging from 20 m to 60 m. Geophysical logging and borehole coring results suggest that the total basalt thickness in the Snake River Plain may exceed three kilometers. A more detailed description of the lithology of the Snake River Plain is given by Knutson et al. [1993].

As our first iteration toward developing a conceptual model for water flow in a fractured basalt vadose zone, we analyzed an extensive data set obtained during the LSIT. The LSIT was an infiltration test conducted at the Radioactive Waste Management Complex of the INEEL in 1994 to characterize water flow on the scale of several hundred meters (the macro-scale) [Wood and Norrell, 1996]. A 26,000 m^2 infiltration basin was flooded with water for a period of 36 days, and several tracers were added to the basin water 6 days after the onset of flooding [Newman and Dunnivant, 1995]. A conceptual model for flow at the macro-scale assumed that the Snake River Plain basalt behaved as an oversized porous medium, in which the network of rubble zones surrounding individual basalt flows represented the pore space and the basalt flows represented the mineral grains. It was assumed that the permeability of the intra-basalt-flow fractures was negligible in comparison with that of the inter-basalt-flow rubble zones. Consequently, the large aspect ratio of the individual basalt flows (lateral extent >> thickness) would impart a large anisotropy to the effective permeability of the medium (horizontal permeability >> vertical permeability).

Because of the anisotropy of the macro-scale model, extensive lateral spreading was expected to accompany infiltration, so a large fraction of the monitoring wells were outside the footprint of the infiltration pond. Of the 101 monitoring locations, water was recovered from 30, and the tracer, Se-75, assumed to be conservative, was found in only 26. No monitoring locations outside the footprint of the infiltration pond showed water or tracer arrival in the vadose zone, except in perched water zones just above a

sedimentary inter-bed located at the depth of approximately 70 m. The shapes of the breakthrough curves varied significantly between the different locations. Newman and Dunnivant [1995] were able to model 10 of the 26 Se-75 breakthrough curves using a one-dimensional model of advection-diffusion transport through a homogeneous porous medium with a constant water velocity. The low success rate of the one-dimensional model indicated that a volume-averaged macro-scale conceptual model was inappropriate for interpreting field-scale measurements within a fractured basalt vadose zone.

In order to interpret the spatial and temporal distribution of tracer in the subsurface, we developed a schematic fracture pattern keyed to representative breakthrough curves from the LSIT (Figure 3). This comparison suggests that the actual arrival time and concentration of tracer reflect the geometric structure of the fracture pattern within the individual basalt flows in addition to that of the rubble zone network. The arrival of tracer depends on the location of the sampling point within the fracture system. The breakthrough curves at individual sampling points have a variety of shapes, depending on the connectivity of the fractures supplying water to that point. Breakthrough curves of this type generally do not allow a unique interpretation of the fracture geometry, but the data shown in Figure 3 confirm the highly complex nature of flow associated with the geometry of the fractured basalt. For example, although tracer-free water infiltrated the basin for six days prior to the addition of tracers, the first water observed in several wells contained tracer (locations 2, 5, and 6). In addition, tracer-free water was observed in several lysimeters throughout the course of the test (locations 3 and 4). Zones where water samples could not be collected were located between water bearing zones. In addition, little correlation between the distance from the tracer source and tracer arrival time was found.

Despite the presence of the inter-basalt-flow rubble zones, lateral spreading was not significant during the LSIT. This indicated that intra-basalt flow fractures contributed considerably more to the overall permeability than had previously been assumed. To better understand this contribution, we focused our studies at the Box Canyon site on the intermediate-scale (several meters) over the central portion of a single basalt flow. At

this scale, the internal fracture pattern within the basalt flow is assumed to be a major factor affecting water flow.

3. Description of the Lithology and Fracture Pattern at Box Canyon

3.1. Lithology

The surface of the Box Canyon site consists of exposed weathered basalt and soils (clays and silts), which infill the near-surface fractures and basalt column joints. The depth to the regional aquifer is about 200 m at the Box Canyon site, and a perched water zone is located at a depth of about 20 m. Along the Box Canyon cliff face, located about 30 m from the infiltration pond, two distinct basalt flows separated by a rubble zone can be seen.

The connectivity of the fracture pattern and its relationship to other geological features are of critical importance. A fracture map provides the best illustration of the fracture spatial distribution, persistence, as well as the size and shape of fracture-bounded blocks [Laubach, 1991]. The map of the fracture pattern in the uppermost basalt flow exposed on the side of the cliff at Box Canyon is shown in Figure 4. The basalt flow is divided into upper and lower zones of distinctly different fracturing, due to different cooling rates and temperature gradients in the upper and lower portions of the basalt flow. As can be seen in Figure 4, many fractures propagate from the outer margins toward the interior of the basalt flow. Fractures of varying length that propagate from the top of the basalt flow connect the surface with horizontal fractures and major vertical fractures. Fractures that propagate upward from the bottom of the basalt flow are less interconnected, and therefore, most may be considered dead-end, or non-conductive, fractures.

Site characterization, including cliff face mapping, borehole logging, and cross-hole gas-phase interference tests, revealed that the fractured basalt vadose zone is comprised of the following geological components shown in Figure 4: (1) soils and flow-top breccia and boulders, (2) near surface soil infilled fractures, (3) upper and lower vesicular zones, (4)

isolated vesicular layers, (5) massive basalt, (6) central fracture zone, and (7) flow-bottom rubble zone.

The discontinuities that affect water flow the most in fractured basalt are column-bounding fractures (also called joints [Engelder, 1987; Priest, 1993]), intra-basalt fractures, fracture zones, and rubble zones. Column bounding fractures in basalt usually form a polygonal network, created perpendicular to the cooling isotherm due to thermal contraction of basalt lava. Using fracture maps of seven basalt flows below and adjacent to the Box Canyon site, we determined the horizontally-averaged spacing between fractures as a function of depth (Figure 5). The spacing between fractures for several basalt flows, likely of the same eruption, is markedly similar, and exhibits an increase in spacing with depth in the upper ~2/3 of the flow thickness. The base of each basalt flow shows an inverted pattern, in which the lower part of basalt flow contains a smaller spacing between fractures than the center of the flow. At the exposed upper surface of the basalt flow, the spacing between fractures is as low as 0.3 meters. However, it is clear that some material has been removed from the upper exposures by weathering, thus removing the basalt with the smallest fracture spacing that is often present in the uppermost 2-3 cm of material in an unweathered basalt flow. Overall, the upper 2/3 of the basalt flow is characterized by small spacing, and thus has more fractures than the lower 1/3. In some basalt flows, there is a region near the center of the basalt flow that contains highly fractured rock that does not display the columnar style of fracturing [Long and Wood, 1986; Tomkeieff, 1940]. These sub-horizontal central fracture zones are present in approximately 40% of basalt flows examined at Box Canyon, and one is observed below the infiltration site (Figure 4).

3.2. Conceptual Model of the Fracture Pattern Geometry

The fracture distribution observed at the Box Canyon cliff face was simplified and idealized in order to construct a simple four-generation tree model shown in Figure 6. The model shows that the largest basalt column is sub-divided into several columns toward the top of the flow. This model also shows the branching (bifurcation)

phenomenon for individual fractures, which may cause preferential flow paths and multiple flow paths leading to a given point.

The model shown in Figure 6 indicates that in order to represent all geological components of a basalt flow, a minimal size for a geological investigation should extend from the top to the bottom of the basalt column, and its width should coincide with the maximum spacing between the columnar joints. At the Box Canyon site, the average spacing between columnar joints is 0.46 m at the surface, 2.0 m near the center of the basalt flow, and 1.3 m at the bottom. The maximum spacing near the center of the flow is from 3.5 m to 4 m.

4. Methods and Results of the Box Canyon Infiltration Tests

4.1. Design of the Box Canyon site

Site Layout and Instrumentation. Over the course of three years, 1995-97, 38 vertical and slanted boreholes (Figure 7) were drilled (diameter 10-15 cm) and logged (natural gamma and caliper measurements, down-hole video recording, borehole scanning, and core description). These data provided information about the types of fractures, the depth of soil infilling the fractures, the occurrence of vesicular zones, and the locations of fracture zones and the rubble zone [Faybishenko et al., 1998a].

The types of instrumentation used during the infiltration tests are summarized in Table 1. A more detailed description of the instrumentation is given by Faybishenko et al. [1998b]. All the instruments were installed in boreholes using the following method of borehole completion [Faybishenko et al., 1998c]. The instruments were attached to the outer faces of polyethylene packers mounted onto sections of 3.5 cm OD PVC manchette pipe, and the sections were glued together to form a continuous string of instruments placed at pre-selected depths. After the string with the probes was lowered into a borehole, the packers and the space between the packers were infilled with polyurethane

resin, thus, pressing the instruments against the borehole walls. This method ensured that water flow did not occur along the borehole walls.

Table 1. Summary of the types of data collected and the instrumentation used during the infiltration test at the Box Canyon site.

Type of Data	Type of Instrumentation	Reference
Cumulative volume of water supplied into the pond	Water flow totalizer	Faybishenko et al., 1998b
Evaporation rate	Evaporation pond	
Local infiltration rates at several locations within the pond	25-cm diameter infiltrometers	Faybishenko et al., 1998b
Water pressure	Tensiometers with water-filled connecting tubes, pressure transducers at the surface	SoilMoisture, Inc., Santa Barbara, CA
Water and tracer samples	Suction lysimeters: single chamber (0-20 ft) double chamber (20-50 ft)	SoilMoisture, Inc., Santa Barbara, CA
Changes in moisture regime	CPN 503DR Hydroprobe	Zawislanski and Faybishenko, 1999
	Time Domain Reflectrometry (TDR) using the Trase System	SoilMoisture, Inc., Santa Barbara, CA
	Ground Penetration Radar (GPR)	Hubbard et al., 1997 Peterson et al., 1997 Vasco et al., 1997
Temperature	Thermistors	Faybishenko et al., 1998b
Electrical resistivity (ER)	Miniature ER probes	Lee et al., 1998
Water level in open boreholes	DTW	Faybishenko et al., 1998b

Based on the geometrical conceptual model of the fracture pattern, we determined that the scale of the infiltration tests should be on the order of 8 m, so that hydrological processes are characterized on a scale that includes at least one or two major column bounding fractures (the maximum spacing between them is 4 m at the center of the flow). Two designs of a 7 m by 8 m pond berm were tested: in 1996, the berm was constructed using bags filled with crushed basalt and injected with polyurethane resin in order to create a watertight barrier. However, this design did not prevent water leakage beneath

and through the berm during the first 1-2 days of the test. For the remainder of the test, the water leakage through the berm to the area outside of the pond was less than 10% of the infiltration rate into the subsurface within the pond. In 1997, a small trench (15 cm high by 15 cm wide) was cut into the basalt at the location of the previous berm and a permanent concrete wall was constructed that practically eliminated water leakage beneath and through the berm.

Design of the Infiltration Tests. A series of ponded infiltration tests was designed to mimic episodic surface-flooding events that occur during large rainstorms or snowmelt events. This is the extreme condition for maximum infiltration and contaminant transport from the surface to the water table.

From 8/27/96 through 9/9/96, a ponded infiltration test (test 96-1) was conducted by maintaining water at a spatially averaged depth of 23 cm above the uneven land surface. A tracer test was conducted midway through test 96-1 by adding a slug of potassium bromide (KBr) to the pond water on 9/2/96, yielding an average tracer concentration in the pond of approximately 3 g/L. The water supply to the pond was halted for two days so the tracer was not diluted; thereafter the water supply was re-established to maintain a constant water level.

A series of four infiltration tests was conducted from 9/11/97 through 11/3/97 (tests 97-1 through 97-4). In each of these tests, a fixed volume of water containing 3 g/L of KBr infiltrated for two days (during test 97-4, the solution infiltrated for four days), and then the remaining solution was pumped out to allow ambient air to enter the subsurface. The purpose of this design was to keep the concentration of the tracer constant in the pond during infiltration. These tests were also designed to decrease the effects of exhaustion processes such as in-washing and swelling of colloids leading to a decrease in the infiltration rate with time, by providing intermittent periods of drying between each test. Periodic flooding is also thought to contribute to a chaotic component of flow in the subsurface, the subject of another investigation being conducted at the Box Canyon site [Faybishenko et al., 1998d]. Table 2 summarizes the volume of water and mass of salt that infiltrated during each test.

Table 2. Summary of volumes of water and masses of tracer (KBr) supplied to the pond during the infiltration tests at the Box Canyon site.

Test	Start of ponding		End of ponding		Volume of water infiltrated (m^3)	Mass of salt infiltrated (kg)
96-1	8/27/96	12:27	9/9/96	11:00	25.00	38.64
97 totals					21.13	63.39
97-1	9/11/97	12:15	9/13/97	12:45	5.42	16.26
97-2	9/18/97	14:56	9/20/97	16:46	5.01	15.03
97-3	10/2/97	15:40	10/4/97	16:00	3.91	11.73
97-4	10/31/97	13:51	11/3/97	15:00	6.79	20.37

4.2. Main Characteristics of Flow and Transport during the Infiltration Tests

Infiltration Rate. To analyze the infiltration rate data obtained in the field, we first determined the cumulative volume of water that infiltrated into the subsurface by subtracting the cumulative volume evaporated from the cumulative volume supplied to the infiltration pond at each time interval. A Horton-type equation was used to fit the data of cumulative volume infiltrated [Jury et al., 1991]

$$q = i_f t + (1/\beta)(i_o - i_f)[1 - \exp(-\beta t)] \quad (1)$$

where

q = cumulative volume infiltrated per unit area (cm^3/cm^2),

t = time (days, from the time when a constant water level was established),

and the fitting parameters are:

i_o = initial infiltration rate (cm/day),

i_f = final infiltration rate (cm/day), and

β = exponential decay parameter.

The experimental data and fitting curves are shown in Figure 8, and the fitting parameters for each test, which were determined using a least square non-linear regression of Horton's exponential function, are summarized in Table 3. Note from Table 3 that in order to compare fitting parameters for all tests, we calculated these parameters for two

cases: (a) assuming that the tests lasted only 2 days, and (b) for the entire duration of tests given in Table 2, because tests 96-1 and 97-4 lasted longer than the other tests.

Table 3. Summary of fitting parameters calculated using Horton's equation (1) fitted to cumulative infiltration data. Note that in 1996, the test was completed in 14 days, whereas the first three tests in 1997 lasted 2 days, and the fourth test lasted 4 days.

Test	96-1		97-1	97-2	97-3	97-4	
duration (days)	11	2	2	2	2	2	4
β (1/day)	0.17	0.12	1.32	4.02	1.17	0.21	0.21
i_o (cm/day)	11.01	10.23	9.96	17.70	6.74	4.05	4.16
i_f (cm/day)	0.00	4.72	2.16	2.70	1.63	3.01	0.63

Horton's equation was derived based on the assumption that exhaustion processes are involved in the reduction of the infiltration rate as the test proceeds [Horton, 1940]. In such processes, the rate of performing work is proportional to the amount of work remaining to be performed. Under ponded conditions, these processes can include surface and fracture sealing due to in-washing, swelling of colloids, redistribution of particles and microbiological clogging. However, numerical simulations of the Box Canyon infiltration test [Doughty, 1999, this issue] showed a decrease in the infiltration rate during ponding even without taking into account near-surface fracture sealing phenomena. We assume that in addition to near-surface fracture sealing, the infiltration rate decreases also due to the following:

1. As water fills the highest permeability vesicular basalt and narrowly-spaced channels in the upper part of the basalt flow, it is funneled to the lower permeability, widely spaced channels in massive basalt in the lower part of the basalt flow, and the overall basalt permeability decreases as the test proceeds.

2. Air redistribution can also affect the decrease in infiltration rate [Faybishenko, 1995] and flow in a fracture [Persoff and Pruess, 1995]. As water moves into partially saturated fractures and imbibes into the matrix, the air it replaces may redistribute itself and block liquid flow paths. During the first six to seven days of test 96-1 and

during the 1997 tests, air bubbles were observed rising to the surface at several locations within the pond.

The infiltration rate, V (cm/day), into the subsurface is given by differentiating Eq. (1) [Jury et. al, 1991]:

$$V = dq/dt = i_f + (i_o - i_f)\exp(-\beta t). \quad (2)$$

Infiltration rates as determined from Eq. (2) are shown in Figure 9 and the fitting parameters are given in Table 3. Although the initial water depths in the pond were the same for all the tests (spatial average of 23 cm), initial infiltration rates varied from 4.1 cm/day to 17.7 cm/day. During test 96-1, the water level was held constant, while during the tests in 1997, the water level dropped 4-6 cm/day. Despite these differences, the final flowrates for all tests converged to a narrow range from 1.6 to 3.0 cm/day. Note that the entire pond surface was water-covered throughout the tests. The decrease in the infiltration rate with time observed in these tests is consistent with the results of many infiltration tests in soils [Jury et al., 1991] and fractured rocks [Kilbury et al., 1986], in which a similar pattern of decreasing the infiltration rate was observed.

Table 4. The standard error and correlation coefficients determined from fitting Horton's cumulative infiltration function to data collected in the field during the four infiltration tests in 1997.

test	Standard error	Correlation coefficient
97-1	0.047	0.9998
97-2	0.083	0.9988
97-3	0.102	0.9962
97-4	0.206	0.9942

Detailed analysis of the infiltration rate (Figure 8 and Table 4) indicated that the measured cumulative infiltration exhibited short-term fluctuations, which increased in magnitude with each successive surface flooding. For example, Figure 8 shows that despite the overall trend of a decrease in the infiltration rate in test 97-4, at the time of 0.7 days the infiltration rate rapidly increased, followed by a period of 0.3 days when the

infiltration rate was practically zero; significant fluctuations were also observed from 1.6 to 1.9 days. Table 4 shows that for each successive test, the standard error increases and the correlation coefficient decreases for the experimental data fitted to Horton's equation. This analysis indicates that the infiltration rate decrease is less monotonic with each successive pulse. Vandevivere et al. [1995] observed that during infiltration tests with microbiological clogging, the hydraulic conductivity of soils may not decrease monotonically, but with fluctuations.

During test 96-1, local infiltration rates were measured with nine infiltrometers (25 cm diameter) within the pond. The water level within the infiltrometers was maintained at the same level as in the pond. The infiltration rates were mostly within the same range as the overall pond infiltration rate, as shown in Table 5. The smallest flux value (infiltrometer #4) was measured at a location where the infiltrometer was installed on the top of a basalt column.

Table 5. Flow rates calculated for individual infiltrometers and the entire pond for 9/2/96 through 9/4/96. Note that these data were calculated using the water level drop at night when evaporation was practically negligible.

Infiltrometer Number	Average flow rate cm/day	Description of surface
1	3.3	soils (2.5 cm)
2	3.6	soils (5 cm) and cracks
3	3.2	soils (5 cm) and cracks
4	0.4	dense basalt
5	1.7	soils (5-15 cm)
6	2.4	soils (30 cm)
7	3.3	soils (15-20 cm)
8	2.4	soils (10-15 cm)
9	1.8	dense basalt
Total in pond	3.1	

Water Pressure. In this section, we analyze the results of field measurements of water pressure using tensiometers from test 96-1 and test 97-3. Measurements were taken at 23 locations between the depths of 0.3 m and 3 m in eight wells within the pond, and three wells outside the pond. Figure 10 shows typical results of water pressure measurements in two boreholes located within the pond. Figure 10a shows that in well T-5, a gradual

response at a depth of 3.04 m underlies no arrival at a depth of 1.52 m, indicating the phenomena of bypass and non-uniform vertical flow. Figure 10b shows that in well T-9, the water pressure decreased after the initial rapid increase at depths of 1.52 and 3.04 m. At the depth of 1.52 m, the water pressure increased again after 7 days. Thus, during test 96-1 a steady-state regime of hydraulic heads did not develop below 0.3 m.

During surface flooding under a constant water level, the water pressure was practically constant with time at all measured locations at the depth of 0.3 m. Thus, the hydraulic gradient from the surface to 0.3 m was also constant with time, despite the decrease in the infiltration rate. This suggests that the decrease in the infiltration rate from the land surface was caused by a decrease in hydraulic properties of the 0.3 m zone including the top soil layer, the near-surface vesicular basalt, and soil-filled fractures.

In contrast to the almost instantaneous response of tensiometers to the beginning of ponding, the pressure responses after the end of ponding occurred much slower. Finsterle and Faybishenko [1998] showed that the tensiometer pressure in fractured rocks is determined by the fracture rock element (fracture or matrix) that is the most permeable at the time of measurements: during the saturation event, the tensiometer measures the fracture water pressure, and during the drying event, it measures the matrix water pressure.

A summary of the changes in water pressure that occurred during tests 96-1 and 97-3 are tabulated in Table 6 for three depth intervals:

1. In the shallow interval (0.3-0.6 m), all the tensiometers showed rapid pressure increases (within 0.5-1 day) during test 96-1, and five of the eight probes showed rapid increases during test 97-3. The three probes that showed no response were already in a wetted formation (indicated by a positive pressure) before the start of test 97-3. They showed no response because under wetted conditions, the arrival of infiltrating water is not necessarily accompanied by a notable pressure increase,

2. In the intermediate interval (1.5-1.8 m), during both tests, some tensiometers responded gradually (within 1 to 3 days) to ponding, suggesting slow, indirect routes of water travel, and

3. In the deep interval (2.7-3 m), there were very few rapid arrivals, and a larger number of non-arrivals, indicating that water bypassed most of the tensiometers.

Table 6. Categorization of the number of tensiometer responses by depth.

Depth	Test 96-1				Saturated
Intervals (m)	Rapid	Gradual	None	Total	before test
0.3-0.6	8	0	0	8	1
1.5-1.8	4	3	1	8	1
2.7-3.0	3	2	2	7	1
Total	15	5	3	23	3
Depth	Test 97-3*				Saturated
Intervals (m)	Rapid	Gradual	None	Total	before test
0.3-0.6	5	0	3	8	4
1.5-1.8	1	3	4	8	2
2.7-3.0	1	1	5	7	1
Total	7	4	12	23	7

*Pressure data from the third test were used because the data records from the other pulses were incomplete due to technical problems with the DAS.

These observations are consistent with the structure of the fracture pattern observed within a single basalt flow, which showed a tributary structure that funnels flow from many shallow fractures to a few fractures as depth increases, as shown in Figures 4 and 6. Lithology at the monitoring point does not correlate well to water arrival time because arrival time depends on the entire flow-path above and below the probe. Tensiometer measurements during test 96-1 in general showed a greater number of rapid increases in pressure than during test 97-3, mostly because the basalt formation was wetter during test 97-3 due to the previous infiltration tests (97-1 and 97-2) and natural precipitation.

Some examples of the vertical hydraulic head profiles determined prior to and during tests 96-1 and 97-3 are shown in Figure 11. If the hydraulic head profile is located to the

right of the diagonal (solid line), the water pressure is positive, and the hydraulic system is saturated or quasi-saturated (with entrapped air). If the hydraulic head profile is located to the left of the diagonal, the water pressure is negative, and the system is unsaturated. In well T-5 during test 96-1 (Figure 11a), the saturated (or quasi-saturated with entrapped air) zone extended from the surface to a depth of about 0.6 m, and the unsaturated zone was present below this depth. However, in the same well during test 97-3, the unsaturated zone extended all the way to the surface (Figure 11b), although conditions were generally wetter in 1997. In well T-9 the formation was saturated (or quasi-saturated) during test 96-1 from the surface to 3 m (Figure 11c), but in test 97-3 there was an unsaturated zone near the surface (Figure 11d). Thus, the presence of an unsaturated zone determined with a local type measurement does not necessarily reflect the overall wetted condition beneath the pond.

Changes in Moisture Regime. Changes in the moisture regime were determined using neutron logging, time domain reflectometry (TDR), and ground penetrating radar (GPR). It appears that the absolute value of the moisture content in fractured rocks cannot be determined from field measurements using these techniques because it is difficult, if not impossible, to obtain calibration curves for fractured rocks [Bishop and Porro, 1996]. Therefore, we examined relative increases in neutron counts and electromagnetic wave travel times to identify zones of increased moisture content and to locate zones of preferential flow.

Based on neutron logging, numerous local increases in moisture content were observed during test 96-1, particularly at depths of 3 m to 4 m and 6.5 m to 8 m (Figure 12). These local moisture content increases indicate preferential flow paths with water bypassing locations above, between, and below these locations. Well R-3, whose neutron logging data is presented in Figure 12, is a slanted well located outside the pond that intersects the vertical projection of the pond at a depth of 12.2 m. The moisture increases above this depth indicate horizontal flow beneath the infiltration pond. The moisture profiles in this deep slanted well prior to and during the tests in 1997 were almost identical to the moisture profiles at the end of test 96-1 [Zawislanski and Faybishenko, 1999].

Apparently the formation was wetted during test 96-1 and did not return to background conditions one year later, before the beginning of test 97-1.

Neutron logging of well T-10 showed that a 1 m zone beneath the pond and a low angle fracture at 1.5 m were wetted sometime during the 1997 tests, while no moisture increase occurred below that depth (Figure 13a). The moisture content at the depth of 1.5 m rapidly increased sometime between tests 97-1 and 97-2, and then increased slowly thereafter (Figure 13b).

Figure 14 shows a wave velocity difference tomogram, obtained using GPR surveys conducted between wells R-1 and R-2 prior to and during test 96-1 [Hubbard et al., 1997; Peterson et al., 1997; Vasco et al., 1997]. There were several local increases in moisture content, especially within the central fractured zone and the rubble zone. During tests 97-1 and 97-2, no significant changes in the moisture content were observed at any depth, confirming results obtained with neutron logging.

TDR probes were installed near the surface to a depth of 0.5 m. All probes within the pond responded almost immediately to ponding, indicating a rapid saturation of both the fractures and matrix at depths down to 0.5 m. These measurements suggested that the near-surface weathered basalt acted as a porous medium. Probes located outside the pond responded later during the infiltration test, indicating lateral movement of water in the near surface zone.

Temperature. Subsurface temperature changes may arise via two modes of heat transfer from the ground surface: conduction caused by temperature gradients, and convection caused by infiltrating water. In a homogeneous medium, temperature changes due to conductive heat transfer with a periodically varying surface temperature are dampened exponentially with depth and delayed in time. Using subsurface temperature profiles collected from Box Canyon [Long et al., 1995], conduction theory predicted that daily temperature variations could propagate only about 0.5 m, while seasonal temperature variations could propagate to a depth of 10 m. Departures from this general pattern

indicate that convection is altering the temperature profile, and potentially could be used to locate preferential flow paths.

During test 96-1, subsurface temperature measurements were for the most part consistent with purely conductive heat flow: temperature changes generally decreased with increasing depth and no thermistor deeper than 7 m showed any temperature change. Of the 29 thermistors used to conduct measurements, seven showed changes in temperature that cannot be explained by conduction alone. Six of the seven were gradual changes in temperature that differed from conduction theory by at most a few degrees. The strongest evidence for convective flow occurred at a depth of 4.6 m in well I-3, where the temperature response showed small daily temperature variations at a depth far too great to be explained by conduction, strongly suggesting that a fast flow path for infiltration was nearby.

During the tests in 1997, all the temperature observations were consistent with conductive heat flow, probably due to the smaller volume of water infiltrated and the wetter pre-test conditions. Both of these factors would lessen the thermal signature of the infiltrating water. A smaller volume of infiltrating water will more readily reach the ambient subsurface temperature, especially if infiltration occurs through isolated preferential flow paths with large surface areas. Subsurface heat capacity increases significantly with increased water content, enhancing the ability of the subsurface to eliminate the temperature difference of the infiltrating water.

Perched Water Levels. Observations using tensiometers installed in backfilled boreholes showed that at some locations the water pressure became positive during ponding (from 0.15 to 1.85 m), indicating that local perched water zones were formed due to infiltration. Perched water zones were also identified in open boreholes within the footprint of the pond. For example, the height of water above the bottom of well T-10 was 0.65 m, and 0.35 m in well T-8A. During test 96-1, seepage of water was observed along the borehole wall at the level of the rubble zone (about 12 m depth) in wells II-7 and II-2. Water also accumulated at the bottom of well II-6 at the depth of 12 m. Wells II-2, II-6, and II-7 are open, uncased wells located 3-5 m NW, E, and SE, respectively,

from the infiltration pond (see Figure 7). Their spatial distribution suggests that lateral flow in the rubble zone was widespread. However, not all of the open wells outside the pond showed perched water at the rubble zone depth, indicating that lateral flow was not uniformly distributed away from the infiltration pond.

During the tests in 1997, perched water was observed in well I-5 (a 12 m deep well located 1.5 m from the boundary of the pond) with an almost immediate rise in the water level during ponding, and then a dramatic drop during periods of drying (Figure 15a). This indicates that there was a major fast flow path linking the pond with the borehole. Note that transient water level changes in conventional boreholes installed in fractured rocks are not quantitative indicators of in situ conditions, because of the different specific yield (S) for the fractured rock ($S << 1$) and the open space ($S=1$) of a borehole (Figure 15b). Thus, our water level observations confirmed that open boreholes in fractured rocks could lead to misleading results. Even if multiple perched water zones were present in fractured basalt (which could greatly enhance the lateral movement of water), these perched water zones might not be observed using conventional water level measurements. It should be noted that uncased boreholes could provide short-circuits between otherwise unconnected fractures.

Water and Tracer Sampling. During the first week of test 96-1 (before the tracer was added), water samples were taken to determine the water arrival time at different depths. Table 7 shows the decrease in the percentage of locations (from 82% to 44%) of water arrival with depth through the upper half of the basalt flow (down to 5 m), which is due to the increase in the fracture spacing with depth. These data are also consistent with the tensiometer data (Table 6), and support the hypothesis of a funneling of flow with increasing depth. There is an increase in the percentage of locations showing water arrival near the central fracture zone (73% within the 5 m to 9 m interval) and rubble zone (67% within the 9 m to 14 m interval) because these zones allow both lateral and vertical flow to occur more easily. The first arrival times given in Table 7 show rapid movement of water, on the order of 5 m/day through the fastest flow paths. However, there were locations at every depth that did not respond during the test.

Table 7. Categorization of water arrival data by depth obtained using suction lysimeters during the 1996 test.

Depth Intervals (m)	Number of locations where water arrived*	Total number of locations sampled	Percent of locations showing water arrival	First arrival time (days since start of test)
0-1	9	11	82	<1 day
1-2	7	10	70	<1 day
2-3	6	9	67	<1 day
3-5	4	9	44	<1 day
5-9	8	11	73	1 day
9-14	4	6	67	2 days
Total	38	56	68	

*During 11 days of monitoring

We determined that lithology at the monitoring location is not an accurate predictor of water arrival measured with suction lysimeters, because whether or not water arrives depends on the entire pathway from the ground surface to the space around the lysimeter. Early arrivals require a relatively direct pathway from the surface to the monitoring location along fractures. The suction lysimeter is not a point-type probe, because as vaccuum is applied, water is drawn from a certain rock volume around the probe. Once the moisture content of fractures and matrix changes, the radius of influence changes as well.

The tracer arrival data from test 96-1 were consistent with water sampling and tensiometry data, suggesting that no single tracer front moved uniformly downward during infiltration. The tracer was detected in lysimeters installed in the rubble zone at depths of 10.5 m and 12 m, and in the fracture zones (or individual fractures) at depths of 2.6 m, 5.5 m, 7.2 m, and 10.1 m. Tracer arrival data suggested that the tracer moved non-uniformly downward during infiltration, re-enforcing the hypothesis of preferential water flow.

Tracer data from the tests in 1997 are for the most part consistent with tracer data from test 96-1. Figure 16 illustrates breakthrough curves for bromide obtained at different depths in well I-1. The wetter conditions and larger mass of tracer introduced during these tests (see Table 2) allowed the tracer to penetrate deeper into the formation than

during test 96-1. At a depth of 1.5 m, bromide concentrations reached over 2 g/L, whereas at 0.3 m, located directly above this point, the concentrations remained at background levels (less than 0.05 g/L), showing strong evidence of preferential flow. A tracer concentration of 0.43 g/L was detected at a depth of 10.1 m, where a horizontal fracture was identified in the lithological log. This indicated that the tracer eventually reached this depth and that the solution was diluted significantly as it infiltrated through the partially saturated fractured basalt, possibly due to an indirect flow path, mixing at fracture intersections, and/or diffusive exchange with liquid in dead-end fractures.

Electrical Resistivity. Miniature electrical resistivity (ER) probes were used to determine localized resistivity values along the boreholes during the infiltration tests. Temporal variations occurred in all tests, usually with decreases in resistivity during ponding (Figure 17a), which we interpret as an increase in tracer (salt) concentration. In general, resistivity values were lower during the tests in 1997 than during test 96-1, because the formation was wetter and/or more saline after the 1996 infiltration test. These results are in agreement with the data obtained from neutron logging, GPR, and tensiometry data.

Nearly all the ER probes (96%) located near fractures or in the central fracture zone showed a decrease in resistivity during the tests in 1997, indicating that the tracer eventually reached most if not all fractures (Figure 17b). 50% of the probes in the rubble zone (~12 m depth), 33% of probes in vesicular basalt, and 30% in massive basalt showed a decrease in resistivity. Thus, the ER measurements showed a qualitative correlation to lithology that was absent in the tensiometer and suction lysimeter measurements (see the discussion of tensiometer and lysimeter measurements above). We assume that because ER probes are sensitive to small changes in tracer and natural ion concentrations, they reacted to small-scale transport phenomena that were not detectable with tensiometer and suction lysimeter measurements.

4.3. Insights from Numerical Modeling of the Ponded Infiltration Test

Numerical modeling was used as a tool to investigate the effects of fracture geometry, lithology, and entrapped air (which cannot be monitored in detail under field conditions)

on water and air velocity fields, infiltration rate, and tracer breakthrough curves. Here we summarize insights into the conceptual model of flow and transport gained from the 2-D (vertical plane) numerical model of test 96-1, described in detail in an accompanying paper by Doughty [1999, this issue]. The spatial discretization for the two-dimensional model (Figure 18a) was created based on the geometry of the fracture pattern and lithology of the exposed Box Canyon cliff face (Figure 4) as well as on borehole lithological data.

Modeling results suggest that the infiltration rate is sensitive to both the intrinsic permeability of the highest permeability features (column-bounding fractures, denoted as primary vertical fractures in Figure 18a) and the functional form of the relative permeability curves used. Despite the fact that this model did not explicitly include a temporal decrease in the hydraulic conductivity of the near-surface layer (see Section 4.2), it showed a temporal decrease in the infiltration rate. These results suggest that the near-surface soil layer is not the only factor controlling the decrease in the infiltration rate, but that the geometry of flow (which results in the funneling effect), the overall decrease in the rock permeability with depth, and entrapped air also contribute to the decrease in infiltration rate.

The model predicted an irregular pattern of flow through the subsurface during the ponded infiltration test, with much of the water flow occurring preferentially through the highest permeability vertical fractures. Short-range lateral flow occurred through vesicular lenses, the central fracture zone, and the rubble zone. Simulation of tracer movement confirmed that a variety of breakthrough curves could be obtained in fractured basalt (Figure 18b), as shown with real data from the LSIT (Figure 3), and from the Box Canyon infiltration tests (Figure 16). Note that the curve numbers in Figure 18b correspond to the location numbers shown in Figure 18a. It can be seen from Figures 18a and 18b that two probes located next to each other (e.g., locations 3 and 4), but representing different lithology, generate different breakthrough curves.

The modeling studies considered two treatments for the air present in the vadose zone [Doughty, 1999, this issue]. In the first case, using the traditional soil physics approach, air is treated as a passive phase, and the model only calculates water flow. In the second case, the vadose zone is considered as a two-phase flow system, in which both water and air flow are simulated. The results suggested that airflow and entrapped air significantly affect infiltration, creating a more non-uniform moisture distribution in the subsurface and decreasing the infiltration rate by about 30%. Examination of gas-phase flow paths showed that while much of the air is purged from the subsurface region below the pond via lateral flow through the central fracture zone and rubble zone, some became entrapped and subsequently flowed upward into the pond through the column-bounding fractures.

5. Summary of the Conceptual Model of Water Flow

The data obtained during the infiltration tests have confirmed that infiltration is primarily controlled by the characteristics of the fracture system within the basalt flow, leading to strongly preferential, irregular and non-repeatable flow patterns in the subsurface. Comparisons between test 96-1 and the tests in 1997 show that flow patterns and zones of saturation are highly variable from test to test. Apparently they do not depend solely on lithological features, but are sensitive to both initial conditions and flow history. Beneath the pond, the basalt may be found in unsaturated, saturated, and quasi-saturated conditions with entrapped air. These phenomena confirm the complex character of water flow in a fractured basalt vadose zone over space and time.

In order to describe such a complex system, we propose the multi-geological-component conceptual model illustrated in Figure 19. This conceptual model recognizes the connections between individual geological components, each with different hydraulic processes governing water flow. Figure 19 shows the main processes of water flow: preferential flow through conductive vertical fractures, fracture-to-matrix diffusion, vesicular basalt-to-massive basalt diffusion, the funneling effect, and lateral flow (along with advective transport) through sub-horizontal fractures and rubble zones. This multi-

geological-component conceptual model is far more complicated than most existing conceptual models for fractured/porous media, such as double-porosity [Barenblatt et al., 1960; Warren and Root, 1963] or triple-porosity [Abdassah and Ershaghi, 1986] models. The simpler models cannot account for all the processes necessary to make accurate predictions of flow and transport in the fractured basalt vadose zone. The key features of our conceptual model are summarized in the following paragraphs.

5.1. Localized, Complex Pattern of Vertical Flow

Pressure measurements and TDR measurements indicated that wetting of the top 0.5 m zone beneath the pond occurred very rapidly. Preferential flow appeared to originate just below this depth, and flow became increasingly localized with increasing depth, as evidenced by the successively fewer instruments responding to ponding. The tree structure of the fracture pattern conceptualized in Figure 6 is consistent with a concept of flow funneling. In this conceptualization, column-bounding fractures provide the primary pathways for fast vertical infiltration. However, the water supply from the surface into column-bounding fractures is restricted due to limited infiltration through sediments filling near-surface fractures. Some fractures terminate within the basalt flow, either creating dead-end flow paths or indirect flow paths composed of linked column-normal and column-bounding fractures. Furthermore, we expect that water flow within initially dry fractures will show the fingering phenomena that have been identified at the laboratory scale [Nicholl et al., 1994; Geller et al., 1996], and with modeling [Pruess, 1998], so even conductive column-bounding fractures will not be uniformly wet. Thus, simply identifying a monitoring point as being located in a vertical fracture does not enable one to predict the flow response, because the response at any point depends on the entire flow path both above the monitoring point, as well as below the monitoring point for non-conductive, dead-end fractures.

5.2. Lateral Flow and Perched Water

Since the largest fractures are vertical, the predominant flow direction under gravity is downward. However, several features such as horizontal fractures connecting terminated vertical fractures, vesicular lenses, the central fracture zone, and the rubble zone promote

lateral flow. If the permeability below the rubble zone is low (likely if the underlying fractures were exposed at the surface for a period of time and are consequently sediment-filled) or if a sedimentary inter-bed occurs there (as at the LSIT, which is typical for the INEEL area), perched water zones can be created and lateral flow can be widespread. Given the high porosity of the rubble zones (presumably up to 50% or higher), the potential for storage of water (and consequently contaminants) is large. Once positive hydraulic pressure is developed within the perched water in the rubble zone, water may migrate upward into dead-end fractures in the lower part of the basalt flow (see Figures 4 and 6), and then from these fractures water can be imbibed into the matrix.

5.3. Infiltration Rate

The decrease in the infiltration rate with time observed in all tests is consistent with the theory and experience of infiltration from the land surface [Jury et al., 1991]. We hypothesize that the main factors affecting the infiltration rate are the topsoil layer, the interface between the soil layer and the fractured basalt, and the near-surface soil-infilled fractures. Small variations of these factors may cause the large range of initial infiltration rates for the tests. We showed in Section 4.2 that the tendency for a pulse-like infiltration rate was observed during test 97-4. We hypothesize that water will penetrate into horizontal fractures only if a critical hydraulic pressure is reached, at which point a hydraulic connection between column-bounding fractures is established. Before the hydraulic connection is established, water flow through the fracture may be cut off, but once a hydraulic connection is made, water begins to flow through the fracture producing a rapid, but short-term increase in the infiltration rate, despite the long–term trend of the decrease in the infiltration rate.

Numerical modeling suggests that the presence of air has a significant effect on infiltration rate and subsurface saturation distribution, and the observation of air bubbles rising through the pond confirms that entrapment of air does occur. We hypothesize that entrapment of air within the wetted zone beneath the pond occurred in both the vesicular basalt and the fractures infilled with sedimentary material due to the irregular spatial flow pattern.

5.4. Fracture-Matrix Interactions

The combination of rapid and gradual increases in water pressure observed during the tests suggests that water is redistributed between conducting fractures and vesicular basalt. The presence of dead-end fractures may promote fracture-matrix interaction by providing a long-term source of fracture-transported water to the basalt matrix [Maloszewski and Zuber, 1993]. Multi-modal breakthrough curves that were obtained at the LSIT, the Box Canyon infiltration tests, and using numerical modeling, are evidence of a confluence of water flow through different sets of fractures of varying permeability and geometry. For remediation efforts, there is a need to recognize that contamination removal will occur at vastly different rates from different geologic components of fractured rock. It is expected that contaminant removal will be a diffusion-limited process, i.e., limited by the process of contaminant diffusion from the low-conductivity matrix into fractures, from which it can be extracted during remediation, for example, using vacuum extraction or a pump-and-treat approach.

6. Conclusions and Future Research

The hydrogeological paradigm that has been used for the past decades has been to collect the most accurate, representative measurements possible, generally over a relatively small area, and then scale up this information to describe the overall behavior of the system. This approach, although it collects very detailed information, effectively limits the overall number of samples because of the expense of manufacturing, calibrating, installing and maintaining a monitoring system. The data from the intermediate scale infiltration tests conducted at Box Canyon combined with those from the LSIT [Newman and Dunnivant, 1995; Wood and Norrell, 1996], showed that it is impossible to identify *a priori* which fractures will transmit water during an infiltration event, implying that much of the monitoring network will be unused. Instruments that do respond will likely be sparsely distributed, and their responses difficult to interpret in terms of the scale of the contamination problem as a whole.

Therefore, our approach to the development of a conceptual model of water flow in a fractured basalt vadose zone is based on a combination of the lithological information and fracture pattern data together with the results of the infiltration tests. The scale of the Box Canyon experiment was chosen to be relevant to both the scale of geologic variability and the scale of contamination problems, for example, leakage from a single tank.

Even with the geology-based, relevant-scale approach we use, it is impossible to obtain a complete, integrated picture of the movement of water within the multi-porosity system of massive and vesicular basalt and fractures partially infilled with sediments. Point measurements cannot be reliably interpolated for such heterogeneous systems, and geophysical measurements are not of high enough resolution to identify individual preferential flow paths. However, by using a combination of these methods, we can make the following observations. From analysis of the geological setting, we have determined that the fracture pattern exhibits a general increase in the fracture spacing downward. This fracture pattern enables a funneling of flow into progressively fewer

flow-paths as depth increases, but they may be impossible to locate, and contaminants can move quickly through them. From analysis of the infiltration-test data, we find that the conventional term "water front", commonly used to characterize infiltration in sedimentary material, is irrelevant for infiltration in fractured rocks. Column-bounding fractures are primary pathways for preferential flow from the surface toward the rubble zone at a depth of 10 m to 12 m. The water flow occurs rapidly through the conducting fractures followed by a gradual saturation of the basalt matrix. Some fractures that were saturated at the beginning of the test desaturated thereafter, suggesting that steady state conditions do not develop.

The multiplicity of time scales at which processes occur in different geological components of basalt has important implications for remediation efforts. Cleanup efforts (e.g., vacuum extraction, pump and treat) that involve mostly high-permeability fracture pathways are likely to yield disappointing results, as low-permeability basalt provides a long-term source of contaminants that continually replenishes the fracture network. The infiltration tests created a complicated saturated-unsaturated system in which local perched water zones developed at different depths. Because perched water bodies enable storage of large quantities of contaminated water, they are important targets for remediation. However, without an understanding of their geologic setting, their wide range of behavior makes the design of an effective remediation scheme difficult.

Future investigations for fractured basalt are needed on different scales to place the present work in the context of the hierarchy of scales. On the single-fracture scale, we can investigate the physics of flow in variably saturated fractures in laboratory studies using transparent fracture replicas [Geller et al., 1996]. On the fracture-network scale, we can investigate the fracture connectivity and trajectories of flow. The Box Canyon site, and other smaller sites with fractured rock outcrops, allow monitoring over entire surfaces rather than the point measurements available with boreholes. In order to study infiltration at the macro-scale we would need to investigate how the junction between basalt flows (sub-vertical rubble zones) create fast flow pathways.

It appears that several alternative models can be used to interpret field data [Pruess et al., 1999]. An exciting new area of research involves conceptualizing flow in the fractured basalt vadose zone as a chaotic dynamical system [Faybishenko et al., 1998d; Faybishenko, 1999]. The motivation for this approach is two-fold: in the temporal regime, we recognize that flow through an unsaturated fracture network may be more like a set of dripping faucets than the continuous flow predicted by Darcy's law and Richards' equation. The chaotic behavior of a dripping faucet has been studied in detail [Shaw, 1984], and may provide a basis for modeling temporal aspects of flow in partially saturated fractures. In the spatial regime, we recognize that the funneling effect of water flow through the fracture pattern, in combination with the widespread lateral flow in the rubble zone, provides the combination of processes (contracting and stretching) that are the hallmark of chaotic processes that result in attractors with fractal geometry. The important output provided by such a model is information on how much can be known about the future behavior of a system. For remediation, this means knowing what questions are reasonable to ask, rather than oversimplifying a system to the point of uselessness in an attempt to answer all questions. A chaotic dynamic approach may provide an entirely new paradigm for describing flow and transport behavior in the fractured basalt vadose zone.

7. References

Abdassah, D., and I. Ershaghi, Triple porosity systems for representing naturally fractured reservoirs, *SPE Paper 13409*, 1986.

Barenblatt, G.E., I.P. Zheltov, and I.N. Kochina, Basic concepts in the theory of seepage of homogeneous liquids in fissured rocks, *J. Appl. Math*, 24(5), 1286-1303, 1960.

Bishop, C.W., and I. Porro, Comparison of neutron moisture gauges and a neutron tool for use in monitoring wells, *Ground Water*, 35(3), 394-400, 1996.

Doughty, C., Mathematical modeling of a ponded infiltration test in unsaturated fractured basalt at Box Canyon, Idaho, 1999 (this issue).

Engelder, T., Joints and shear fractures in rock, in *Fracture Mechanics of Rock*, edited by B.K. Atkinson, pp. 27-69, Academic Press, Orlando, FL, 1987.

Faybishenko, B., Evidence of chaotic behavior in flow through fractured rocks, and how we might use chaos theory in fractured rock hydrogeology, in Proceedings of the International Symposium "Dynamics of Fluids in Fractured Rocks: Concepts and Recent Advances," February 10-12, 1999, Berkeley, CA, *Lawrence Berkeley National Laboratory Report LBNL 42718*, pp. 207-212, 1999.

Faybishenko, B., Hydraulic behavior of quasi-saturated soils in the presence of entrapped air: laboratory experiments, *Water Resour. Res.*, 31(10), 2421-2435, 1995.

Faybishenko, B., P. Holland, M. Mesa, D. Burgess, C. Knutson, and B. Sisson, Lithological conditions at Box Canyon site: Results of drilling, coring and open borehole measurements, 1995-1997 data report, *Lawrence Berkeley National Laboratory, LBNL-40182*, September, 1998a.

Faybishenko, B., R. Salve, P. Zawislanski, K.H. Lee, P. Cook, B. Freifeld, K. Williams, and C. Doughty, Ponded infiltration test at the Box Canyon site: Data report and preliminary analysis, *Lawrence Berkeley National Laboratory Report LBNL-40183*, 1998b.

Faybishenko, B., J.B. Sisson, K. Dooley, W.E. McCabe, and H.W. McCabe, New technology for borehole completion in fractured rocks using injection of polyurethane foam, *Lawrence Berkeley National Laboratory Report LBNL-41683,* 1998c.

Faybishenko, B., C. Doughty, J. Geller, S. Borglin, B. Cox, J. Peterson Jr., M. Steiger, K. Williams, T. Wood, R. Podgorney, T. Stoops, S. Wheatcraft, M. Dragila, and J. Long, A chaotic-dynamical conceptual model to describe fluid flow and contaminant transport in a

fractured vadose zone, *Lawrence Berkeley National Laboratory Report LBNL-41223*, 1998d.

Finsterle, S., and B. Faybishenko, What does a tensiometer measure in fractured rocks?, in Characterization and Measurement of the Hydraulics Properties of Unsaturated Media, October 22-24, 1997, Riverside, CA, 1998.

Geller, J.T., G. Su, and K. Pruess, Preliminary studies of water seepage through rough-walled fractures, *Lawrence Berkeley National Laboratory Report LBNL-38810*, 1996.

Heath, R.C., Basic ground-water hydrology, *Water Supply Paper 2220, U.S. Geological Survey, Alexandria, VA*, 1984.

Horton, R.E., An approach toward a physical interpretation of infiltration-capacity. *Soil Sci. Soc. Am. Proc.*, 5, 399-417, 1940.

Hubbard, S.S., J.E. Peterson, E.L. Majer, P.T. Zawislanski, K.H. Williams, J. Roberts, and F, Wobber, Estimation of permeable pathways and water content using tomographic radar data, *The Leading Edge of Exploration*, 16(11), 1623-1628, 1997.

Jury, W.A, Gardner, W.R., and Gardner, W.H., *Soil Physics*, John Wiley & Sons, Inc, New York, NY, 1991.

Kilbury, R.K., T.C. Rasmussen, D.D. Evans, and A.W. Warrick, Water and air intake of surface-exposed rock fractures in situ, *Water Resour. Res.*, 22(10), 1431-1443, 1986.

Knutson, C.F., D.O. Cox, K.J. Dooley, and J.B. Sisson, Characterization of low-permeability media using outcrop measurements, in 68th Annual Technical Conference and Exhibition of the Society of Petroleum Engineers, October 3-6, 1993, Houston, TX, *SPE Paper 26487*, 1993.

Laubach, S.E., Fracture patterns in low-permeability-sandstone gas reservoir rocks in the Rocky Mountain region, in Presentation at the Rocky Mountain Regional Meeting and Low-Permeability Reservoirs Symposium, April 15-17, 1991, Denver, CO, *SPE Paper 21853*, 1991.

Lee, K.H., A. Becker, B. Faybishenko, and R. Solbau, Electrical Resistivity Monitoring Borehole Array. Patent application submitted to the LBNL Patent Department on 7/8/98 (IB-1425), 1998.

Long, J.C.S., J. Remer, C. Wilson, and P.A. Witherspoon, Porous media equivalents for networks of discontinuous fractures, *Water Resour. Res.*, 18(3), 645, 1982.

Long, J.C.S., C. Doughty, B. Faybishenko, A. Aydin, B. Freifeld, K. Grossenbacher, P. Holland, J. Horsman, J. Jacobsen, T. Johnson, K. -H. Lee, J. Lore, K. Nihei, J. Peterson, Jr., R. Salve, J. Sisson, B. Thapa, D. Vasco, K. Williams, T. Wood, and P. Zawislanski,

Analog site for fractured rock characterization, annual report FY 1995, *Lawrence Berkeley National Laboratory Report LBNL-38095*, 1995.

Long, P. and B. Wood, Structures, textures, and cooling histories of Columbia River basalt flows, *Geol. Soc. Am. Bull.*, 97, 1144-1155, 1986.

Maloszewski, P., and A. Zuber, Tracer experiments in fractured rocks: Matrix Diffusion and the Validity of models, *Water Resour. Res.*, 29(8), 2723-2735, 1993.

Newman, M.E. and F.M. Dunnivant, Results from the large-scale aquifer pumping and infiltration test: transport of tracers through fractured media, *Idaho National Engineering Laboratory Report INEL-95/146 ER-WAG7-77*, 1995.

Nicholl, M.J., R.J. Glass, and S.W. Wheatcraft, Gravity-driven infiltration instability in initially dry nonhorizontal fractures, *Water Resour. Res.*, 30(9), 2533-2546, 1994.

Peterson, J.E., Jr., S. Hubbard, K.H. Williams, E.L. Majer, and P. Zawislanski, Moisture content estimation using crosshole radar measurement, *Abstract of the 1997 AGU Spring Meeting*, Baltimore, EOS 78(17), p. S166, May, 1997.

Persoff, P. and K. Pruess, Two-Phase Flow Visualization and Relative Permeability Measurement in Natural Rough-Walled Rock Fractures, *Water Resour. Res.*, *31*(5), pp. 1175-1186, 1995.

Priest, S.D., *Discontinuity analysis for rock engineering*, Chapman and Hall, London, 1993.

Pruess, K., On water seepage and fast preferential flow in heterogeneous, unsaturated rock fractures, *J. Contam. Hydrol.*, 30, 333-362, 1998.

Pruess, K., B. Faybishenko, and G.S. Bodvarsson, Alternative concepts and approaches for modeling flow and transport in thick unsaturated zones of fractured rocks, *J. Contam. Hydrol.*, in press, 1999.

Long, J.C.S., ed., *Rock Fractures and Fluid Flow: Contemporary Understanding and Applications, Committee on Fracture Characterization and Fluid Flow of the National Academy of Sciences*, National Academy Press, Washington D.C., 1996.

Shaw, R., *The Dripping Faucet as a Model of Chaotic System*, Aerial Press, Santa Cruz, CA, 1984.

Tomkeieff, S.I., The basalt lavas of the Giant's Causeway district of Northern Ireland, *Bulletin Volcanolojique*, 2(6), 89-146, 1940.

Vandevivere, P., P. Baveye, D. Sanchez de Lozada, and P. DeLeo, Microbial clogging of saturated soils and aquifer materials: Evaluation of mathematical models, *Water Resour. Res.*, 31(9), 2173-2180, 1995.

Vasco, D.W., Peterson, J.E, Jr., and Lee, K., Ground-penetrating radar velocity tomography in heterogeneous and anisotropic media, *Geophysics*, 2(6), 1758-1773, 1997.

Warren, J.E., and P.J. Root, The behavior of naturally fractured reservoirs, *Soc. Pet. Eng. J., Transactions, AIME*, 228, 245-255, September 1963.

Welhan, J.A., and M.F. Reed, Geostatistical analysis of regional hydraulic conductivity variations in the Snake River Plain aquifer, eastern Idaho, *GSA Bulletin*, 109(7), 855-868, 1997.

Wood, T.R. and G.T. Norrell, Integrated large-scale aquifer pumping and infiltration tests: groundwater pathways OU 7-06: summary report, *Idaho National Engineering Laboratory Report INEL-96/0256*, 1996.

Zawislanski, P.T. and B. Faybishenko, New casing and backfill design for neutron access boreholes, *Ground Water,* 37(1), 33-37, 1999.

8. Acknowledgments

Contributions to the design of the tests and numerous discussions with Buck Sisson, Kirk Dooley, and Tom Stoops of the INEEL, and Kenzi Karasaki and others of LBNL are very much appreciated. Rohit Salve, Marque Mesa and Ryan Nelson participated in fieldwork and preliminary data analysis. Scott Mountford conducted analytical analyses of water samples. Ken Grossenbacher and Preston Jordan of LBNL participated in geological investigations. P. Rizzo, R. Solbau, D. Lippert, and J. Clyde participated in the design and fabrication of field instrumentation. Reviews by G. Moridis, T. Tokunaga, and J. Wang of LBNL and R. Podgorney of INEEL are very much appreciated. This work was funded by the Office of Environmental Management, Office of Science and Technology, Characterization, Monitoring, and Sensor Technology Crosscutting Program of the U.S Department of Energy, under Contract No. DE-AC03-76SF00098.

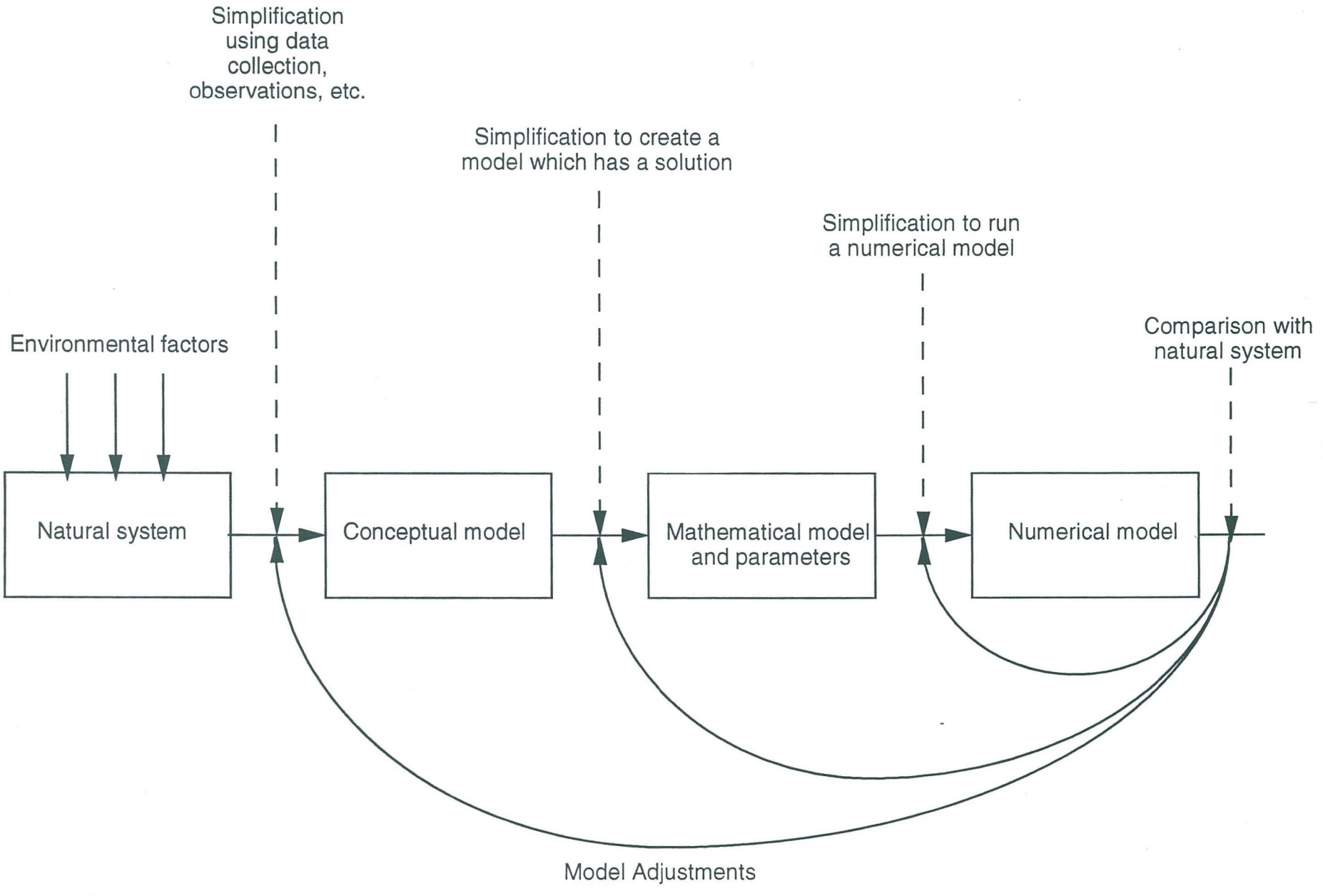

Figure 1. The relationship between different stages of an investigation showing how a conceptual model relates to field and numerical investigations.

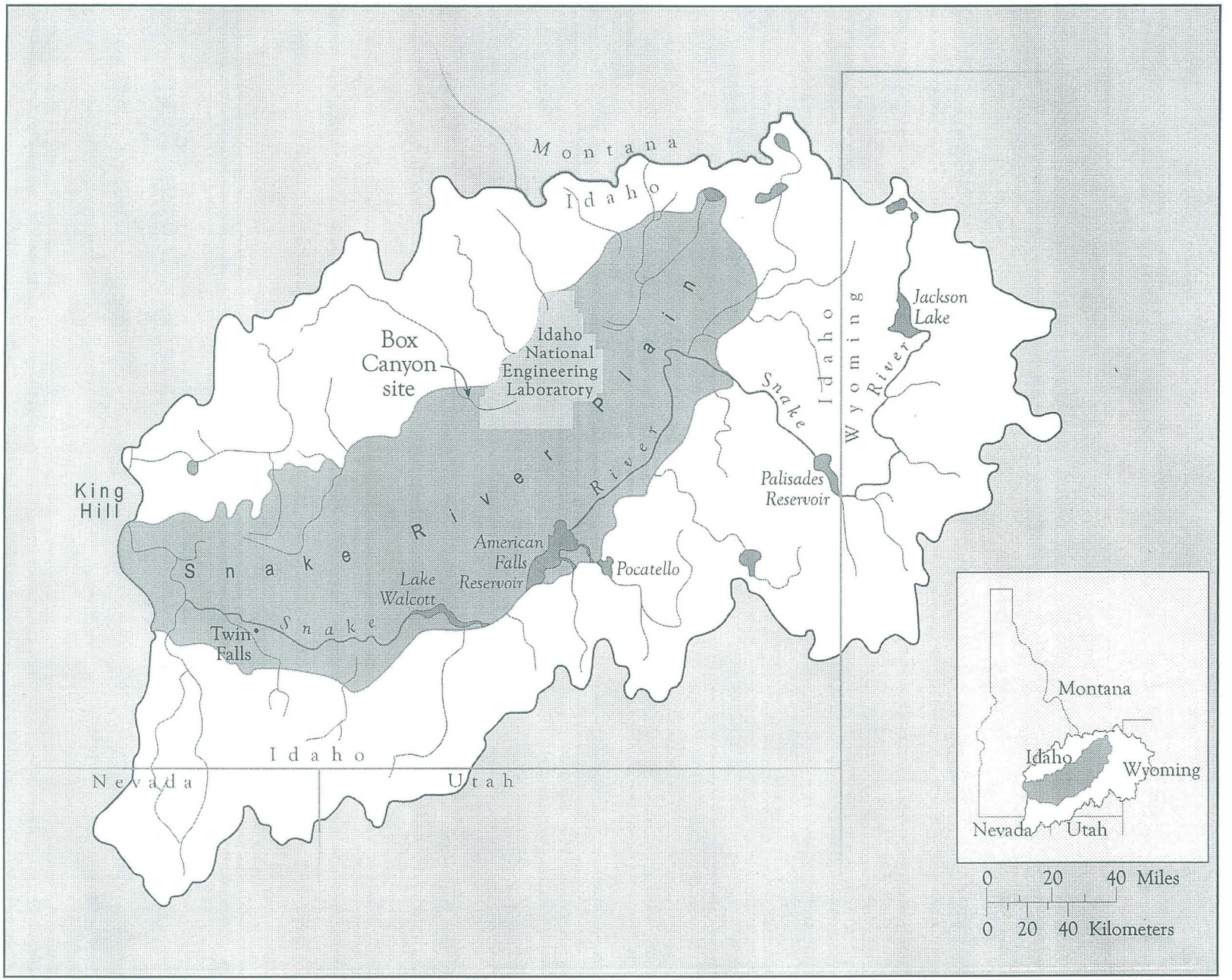

Figure 2. Map of the East Snake River Plain and the location of the Box Canyon experimental site.

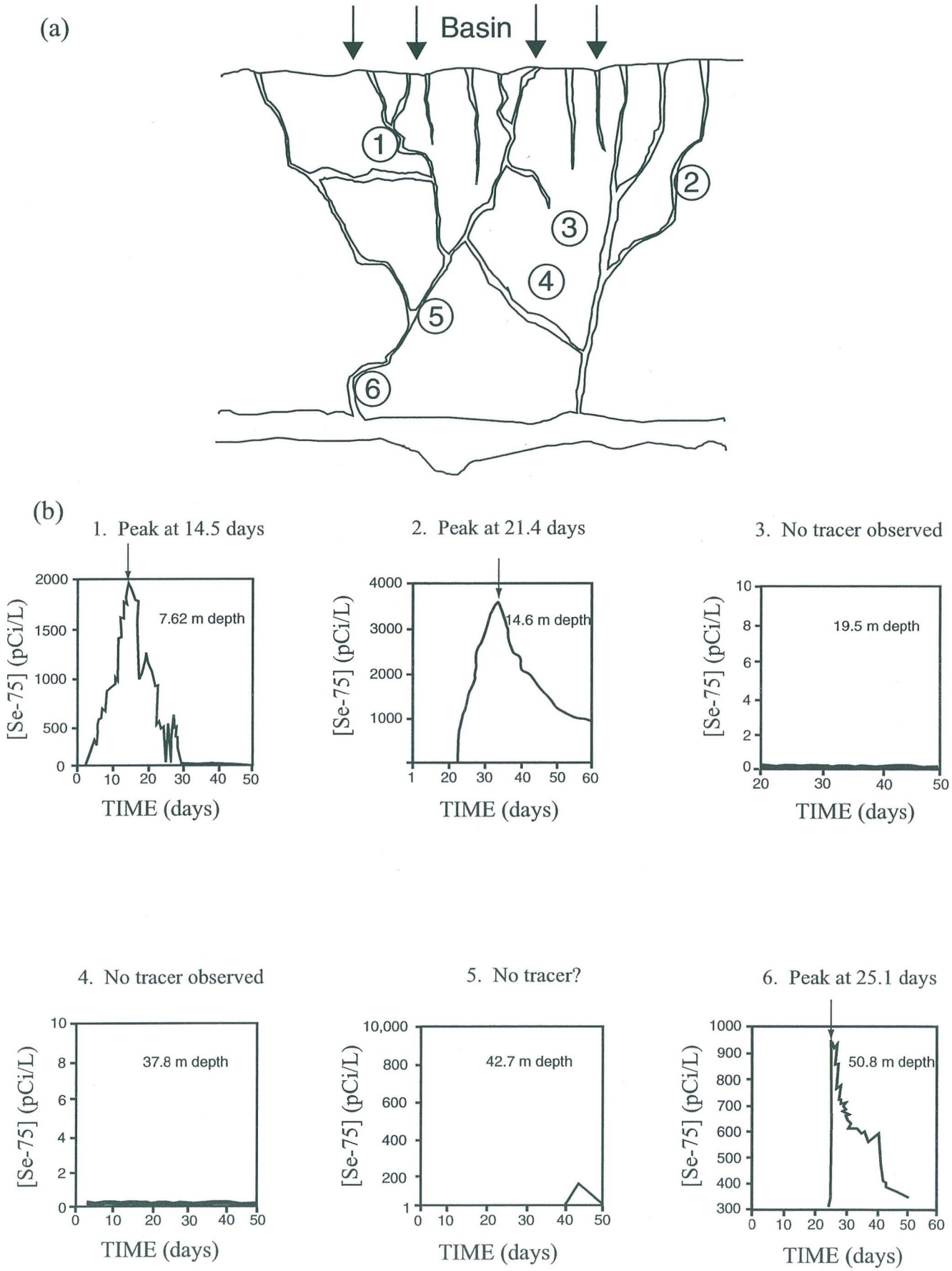

Figure 3. A conceptual model of a fracture pattern (not to scale) and the types of flow paths (a), and different tracer breakthrough curves (b) determined during the LSIT. The numbers on (a) indicate the locations of lysimeters for which breakthrough curves are shown: (1) multi-modal BTC due to a confluence of flow from multiple conductive fractures, (2) single-peak BTC in a single conductive fracture, (3) very slow diffusion of the tracer in a saturated dead-end fracture, (4) no-tracer arrival in a low permeable massive basalt, (5) diffusion of the tracer in vesicular basalt near a conductive fracture, and (6) delayed and abrupt tracer arrival in a deep horizontal fracture or rubble zone.

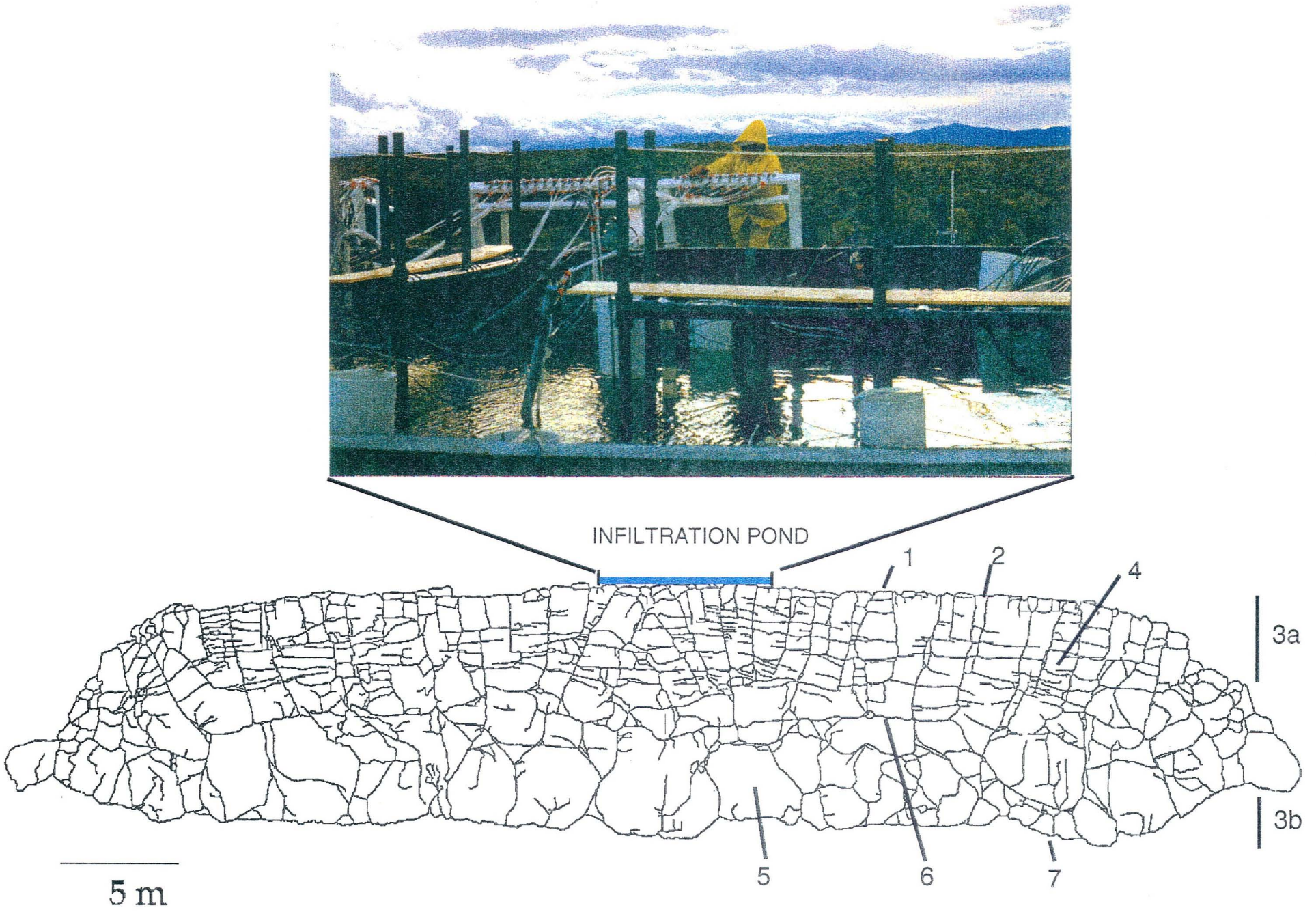

Figure 4. Map of the fracture pattern at the basalt outcrop at Box Canyon, showing the main functional geological components affecting water flow: (1) soils and flow-top breccia and boulders, (2) near surface soil infilled fractures, (3) upper and lower vesicular zones, (4) isolated vesicular layers, (5) massive basalt, (6) central fracture zone, and (7)

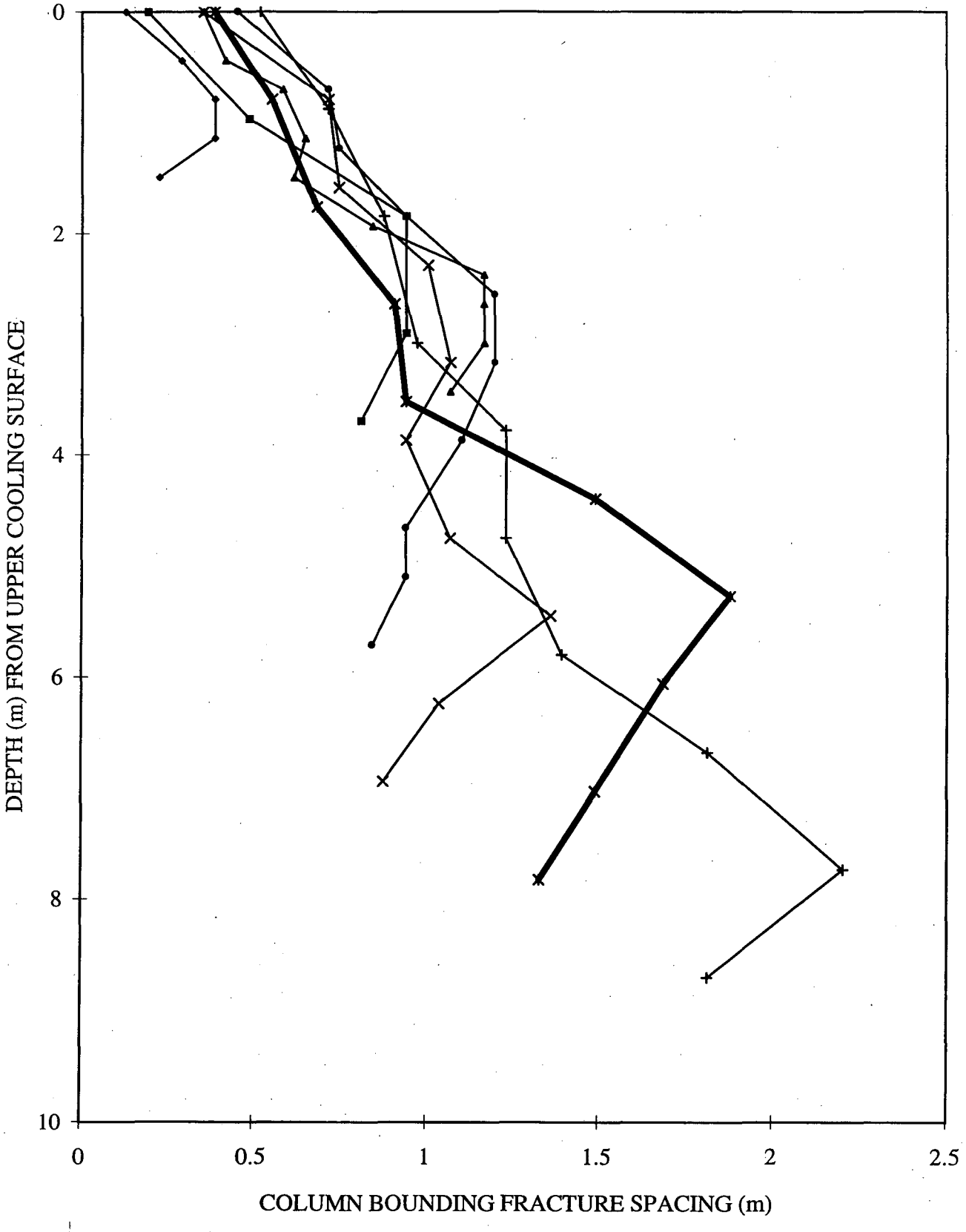

Figure 5. Column-bounding fracture spacing as a function of depth for seven basalt flows under (thick line) and adjacent to the Box Canyon infiltration pond.

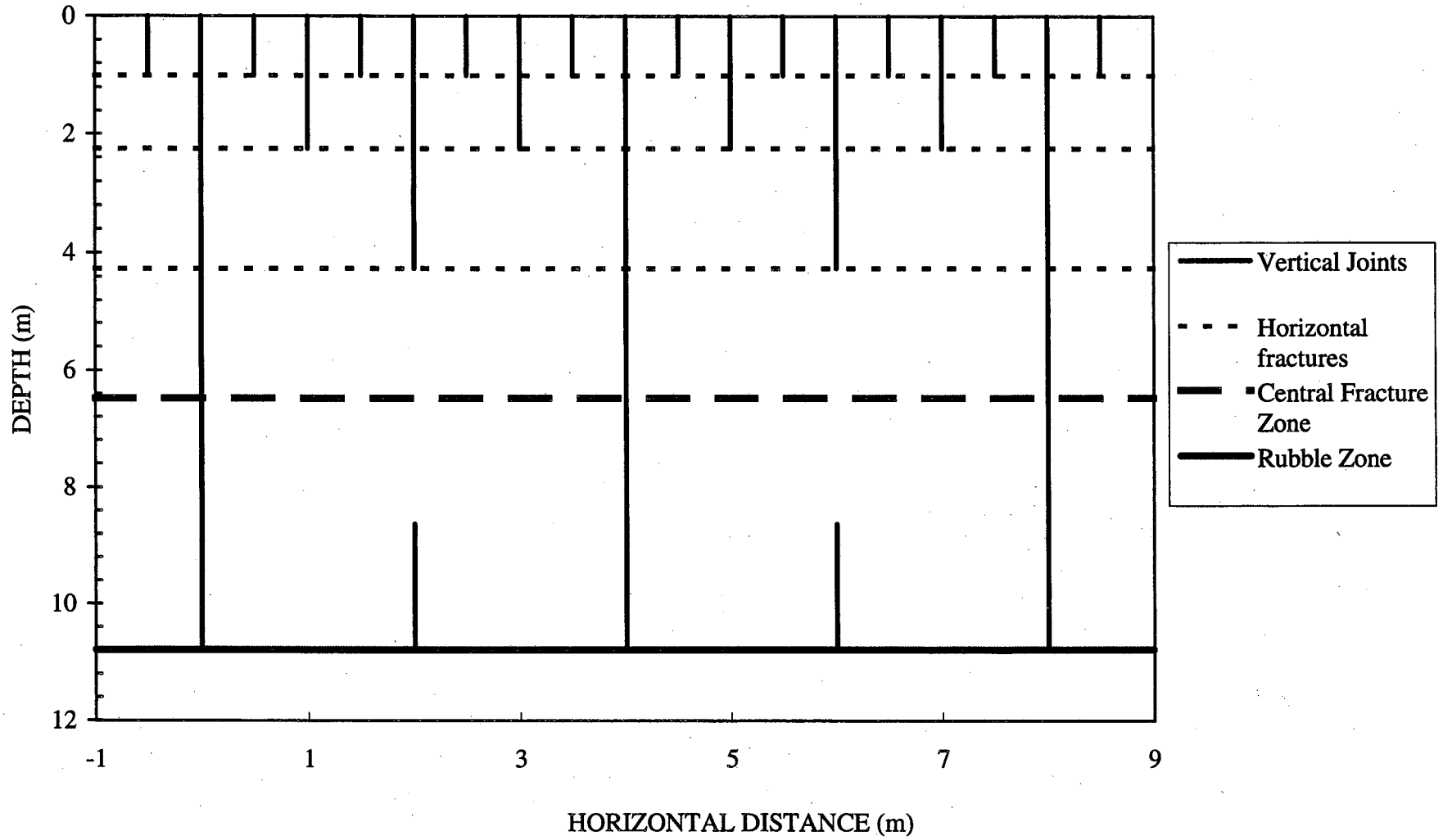

Figure 6. A conceptual tree-type model of the fracture pattern and fracture connectivity of the basalt flows. Note that non-conductive fractures are not shown.

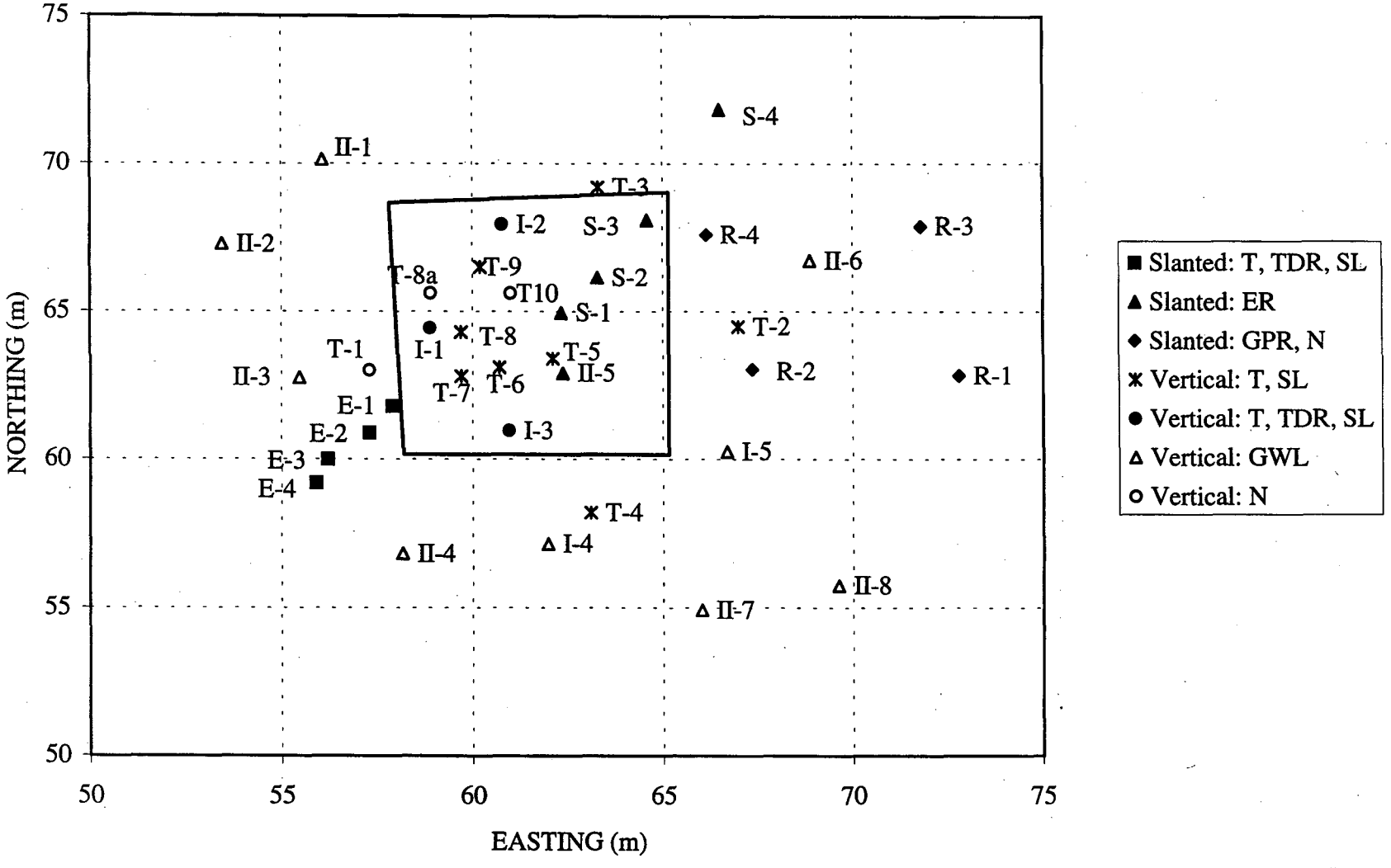

Figure 7. A map of the Box Canyon field site showing the well layout and the infiltration pond. The legend shows the orientation of the wells (vertical or slanted), types of instrumentation installed, and measurements taken: water pressure with tensiometers (T), water sampling with suction lysimeters (SL), electrical resistivity (ER), time domain reflectometry (TDR), ground penetrating radar (GPR), ground water level (GWL), and neutron logging (N).

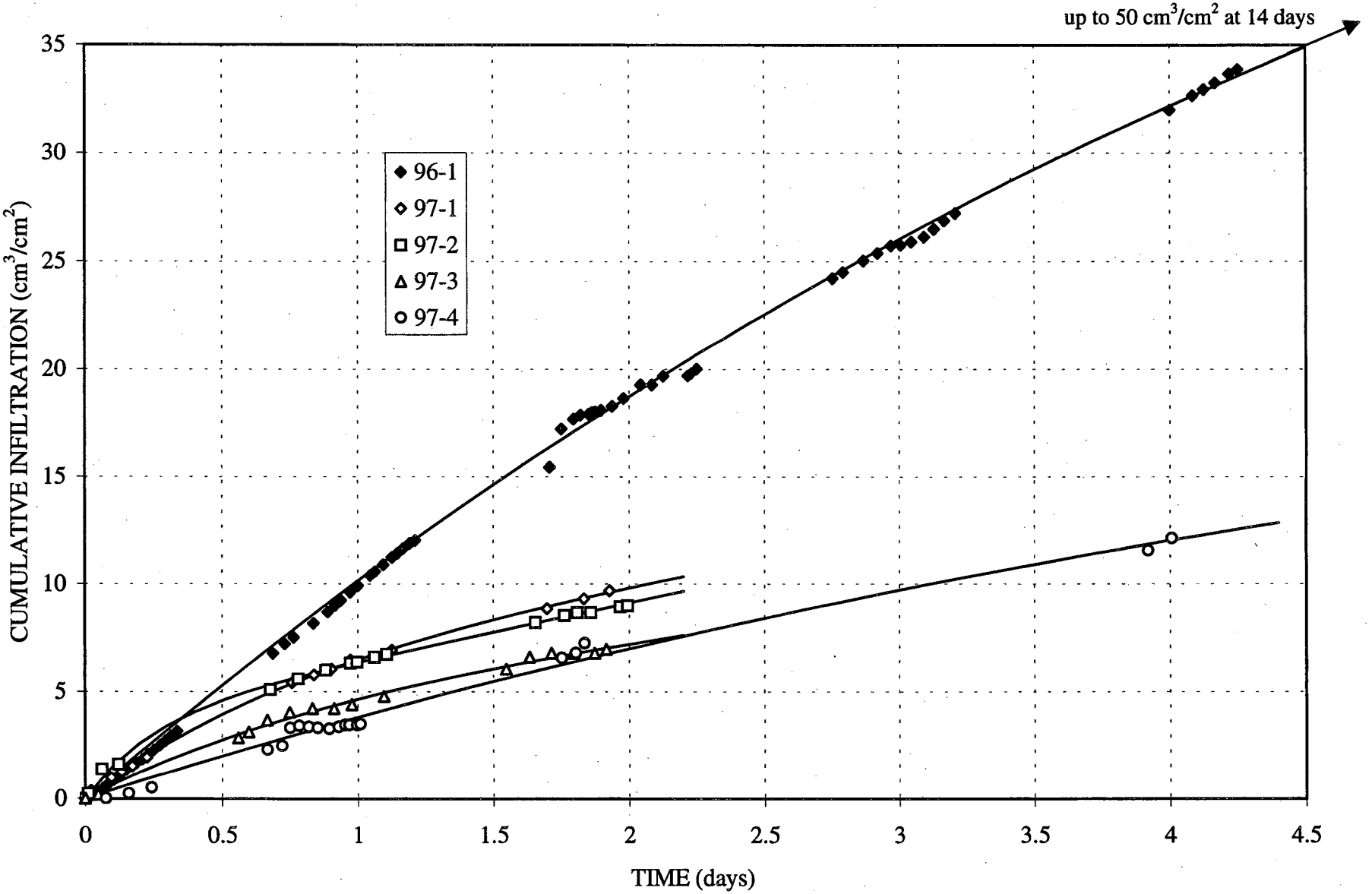

Figure 8. Time variation of the cumulative total volume of water infiltrated during the tests. The fitted lines are from a regression analysis using Equation (1). Test 96-1 was conducted for 14 days, however only 4.5 days are shown.

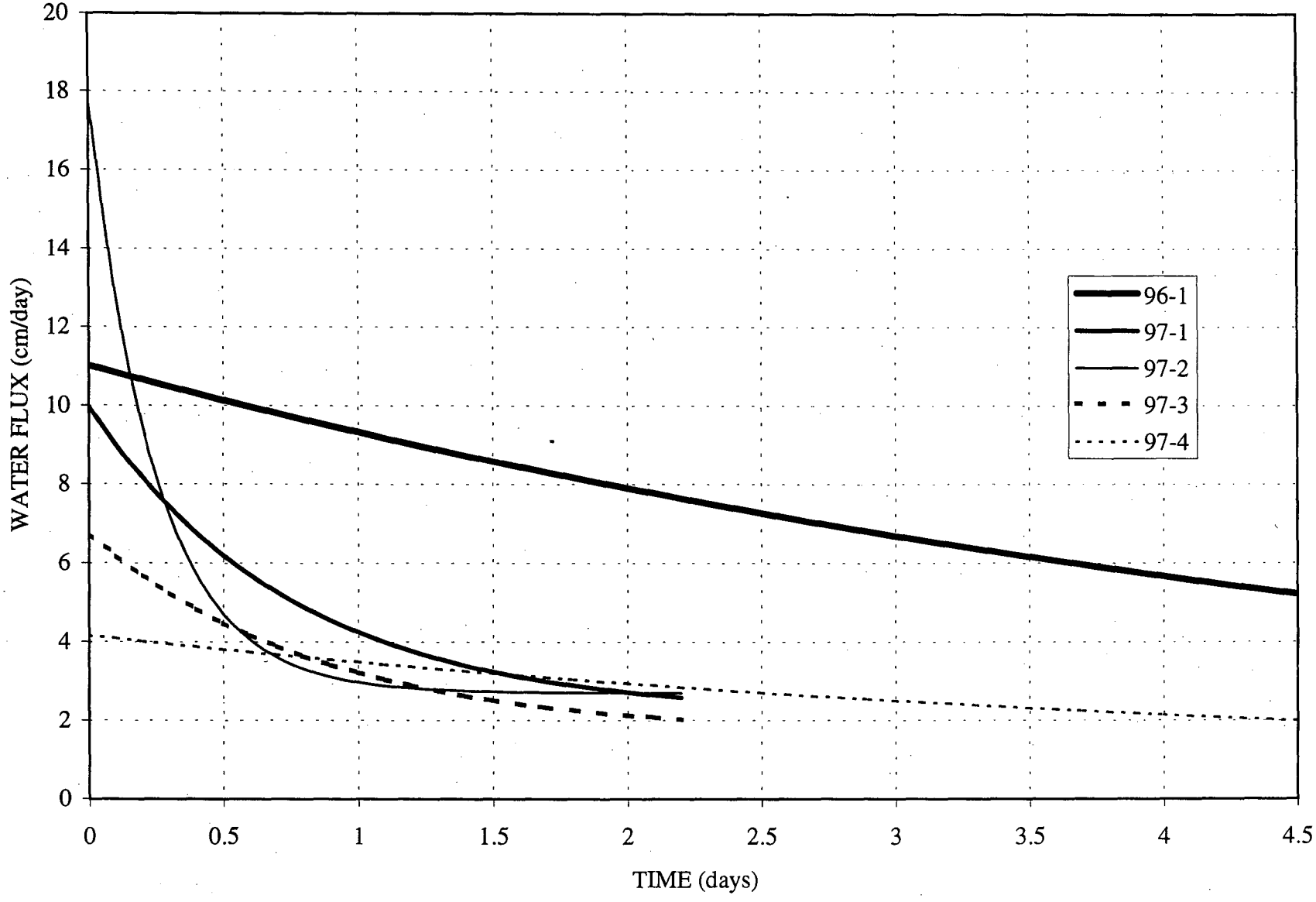

Figure 9. Time variation of the infiltration rates as determined from the derivative of the cumulative infiltration curves using Equation (2).

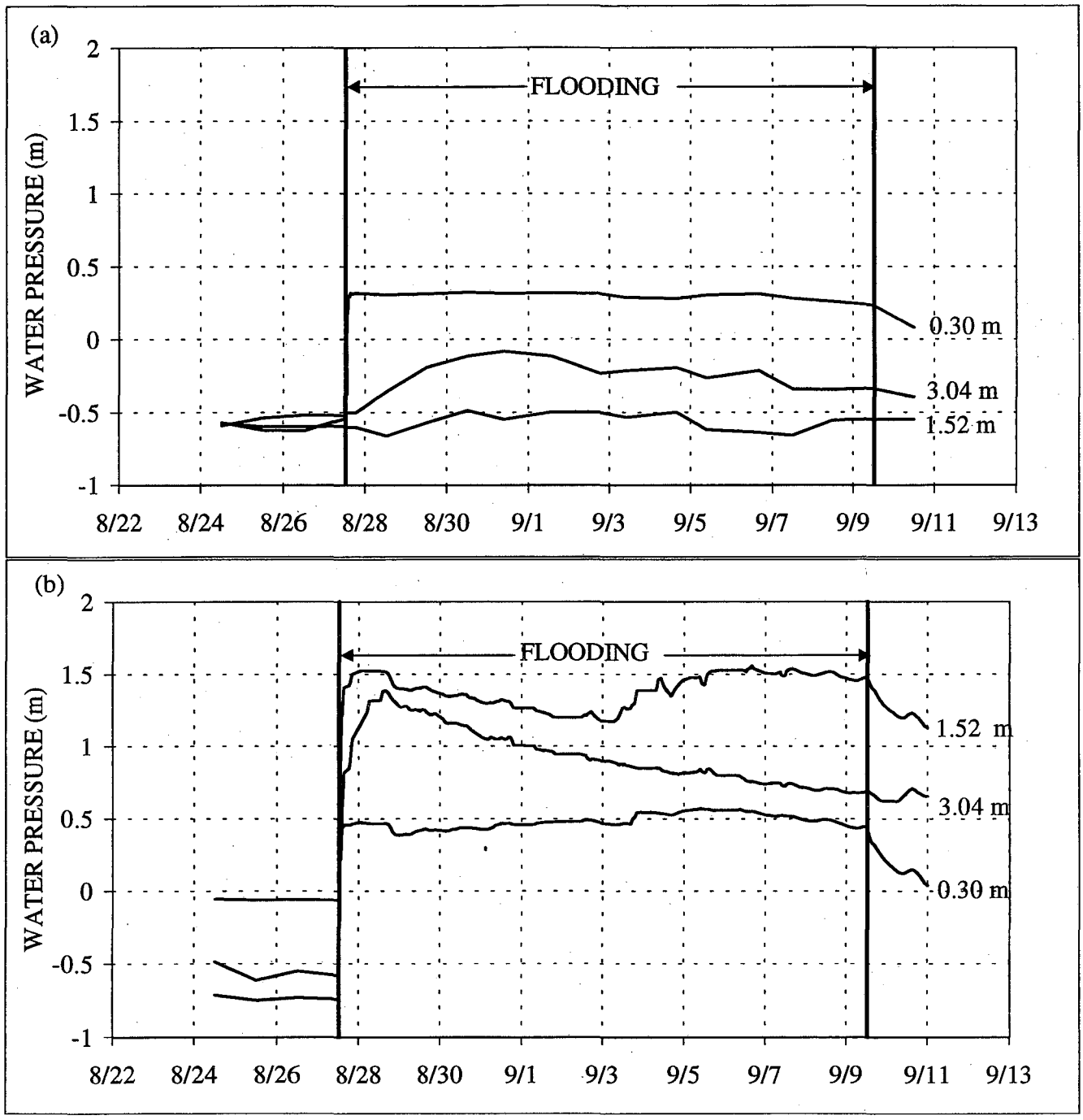

Figure 10. Time-trend of water pressure measured with tensiometers in boreholes at different depths before and during test 96-1: (a) well T-5 and (b) well T-9. Note that daily averaged pressures are shown before the test and in well T-5 during the test at depths of 1.52 m and 3.04 m because pressure fluctuations were large due to temperature fluctuations. Otherwise, nine-point averaged pressures are shown.

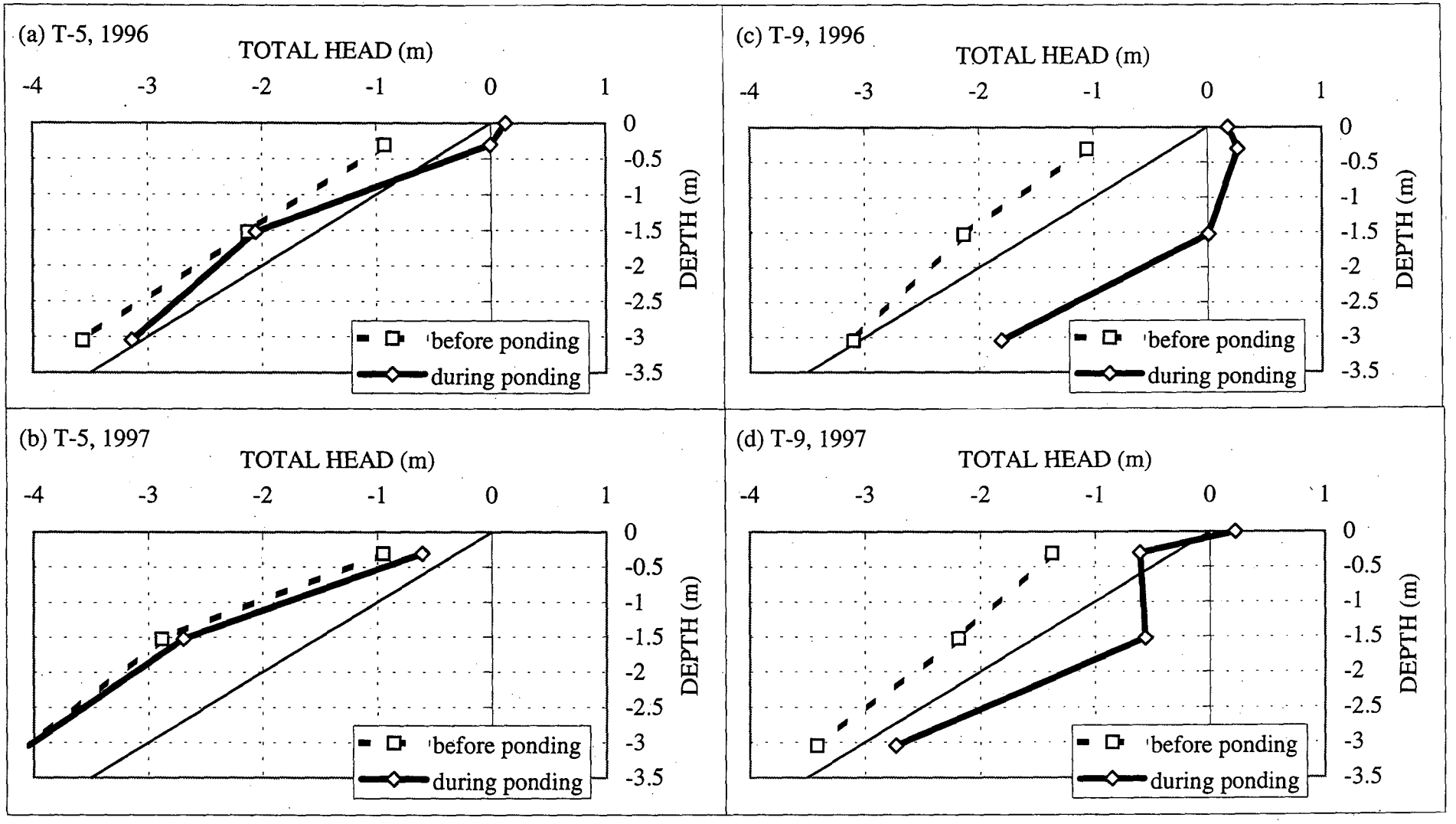

Figure 11. Hydraulic head variations with depth in wells T-5 and T-9 before and during the infiltration tests: (a) well T-5, test 96-1; (b) well T-5, test 97-3; (c) well T-9, test 96-1; (d) well T-9, test 97-3.

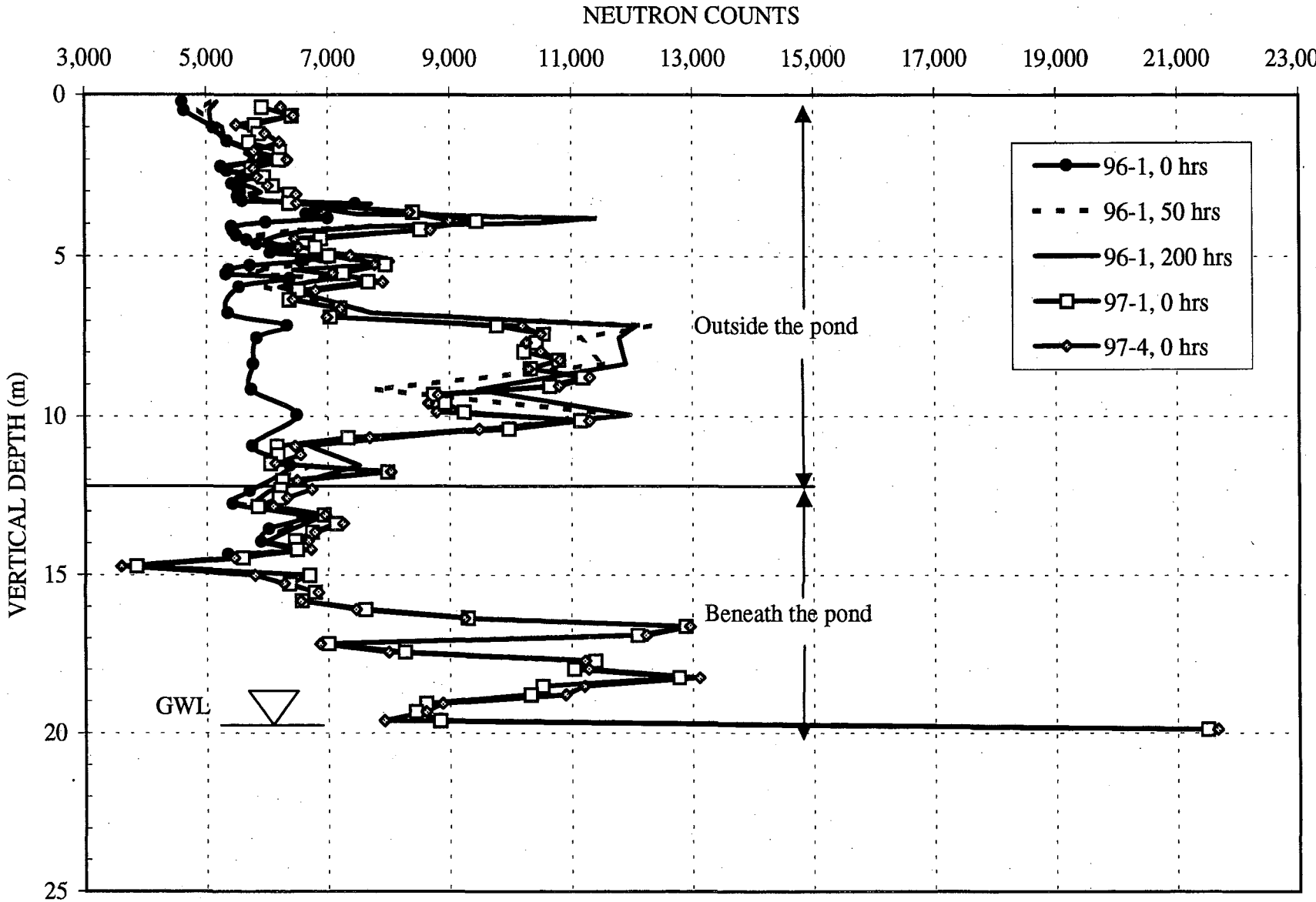

Figure 12. Neutron logging results in well R-3, a slanted borehole located partially (from the surface to the depth of 12.2 m) outside of the pond, and partially beneath the pond, before and during test 96-1 and the tests in 1997. Note that the groundwater level is at 19.8 m. An increase in neutron counts is interpreted as an increase in moisture content.

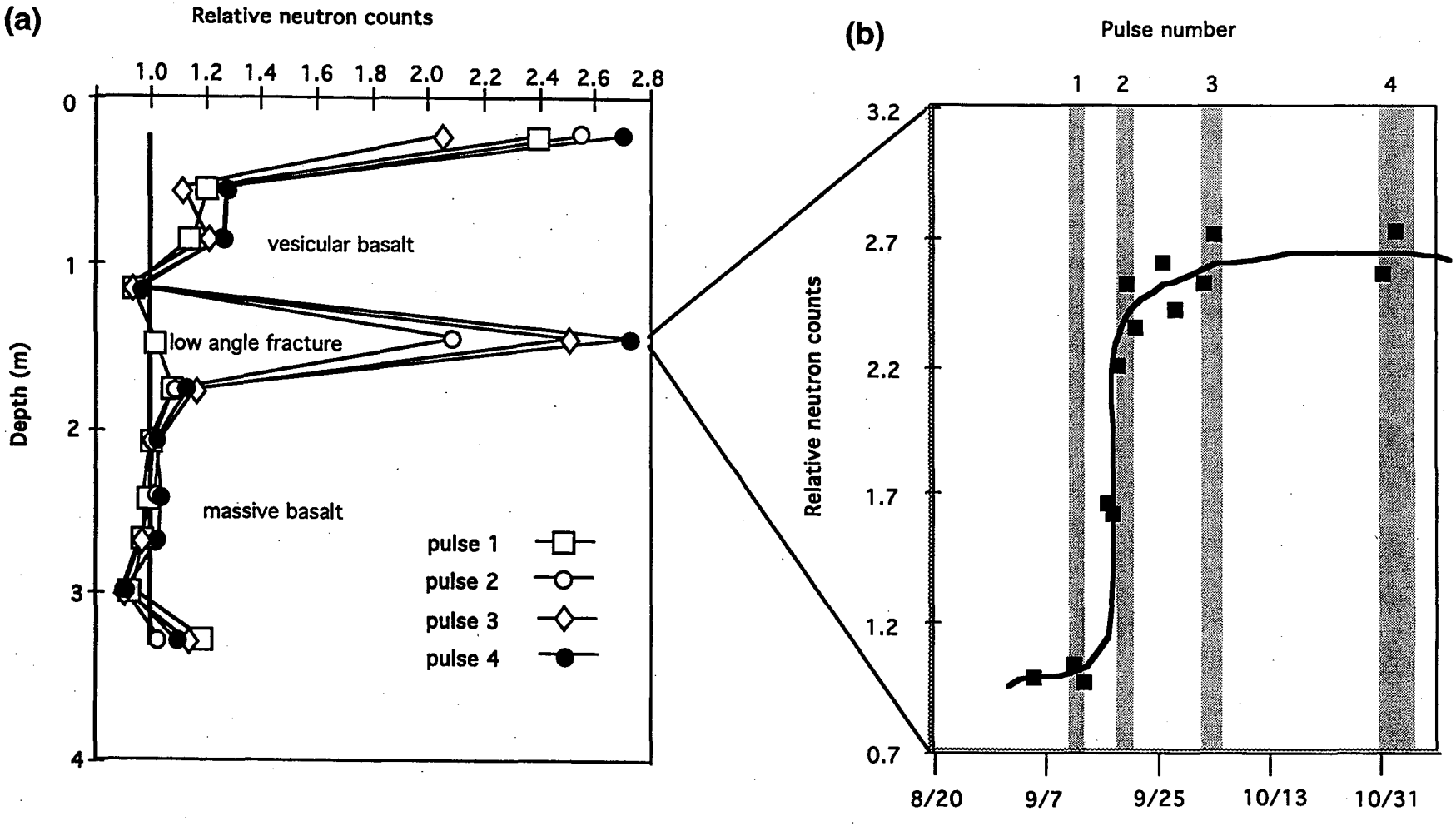

Figure 13. Neutron counts relative to pre-test counts in well T-10, a vertical borehole located inside the pond, during the 1997 tests: (a) vertical profile, (b) temporal change at 1.5 m.

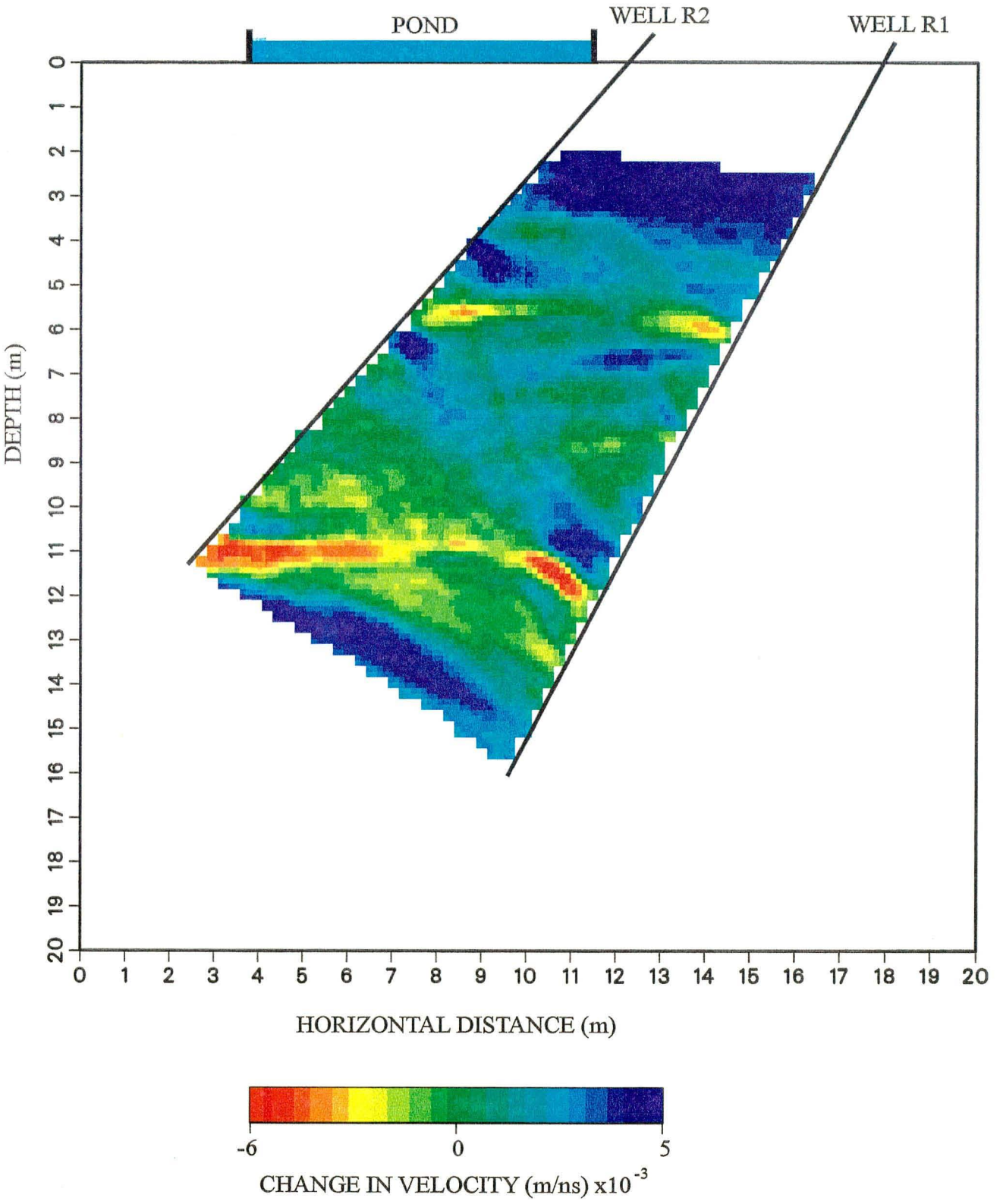

Figure 14. A wave velocity difference tomogram obtained from GPR surveys conducted prior to and during test 96-1. Note that a decrease in velocity, which is represented by the red and yellow areas on the figure, are interpreted as increases in the moisture content [Hubbard et al., 1997; Peterson et al., 1997; Vasco et al., 1997].

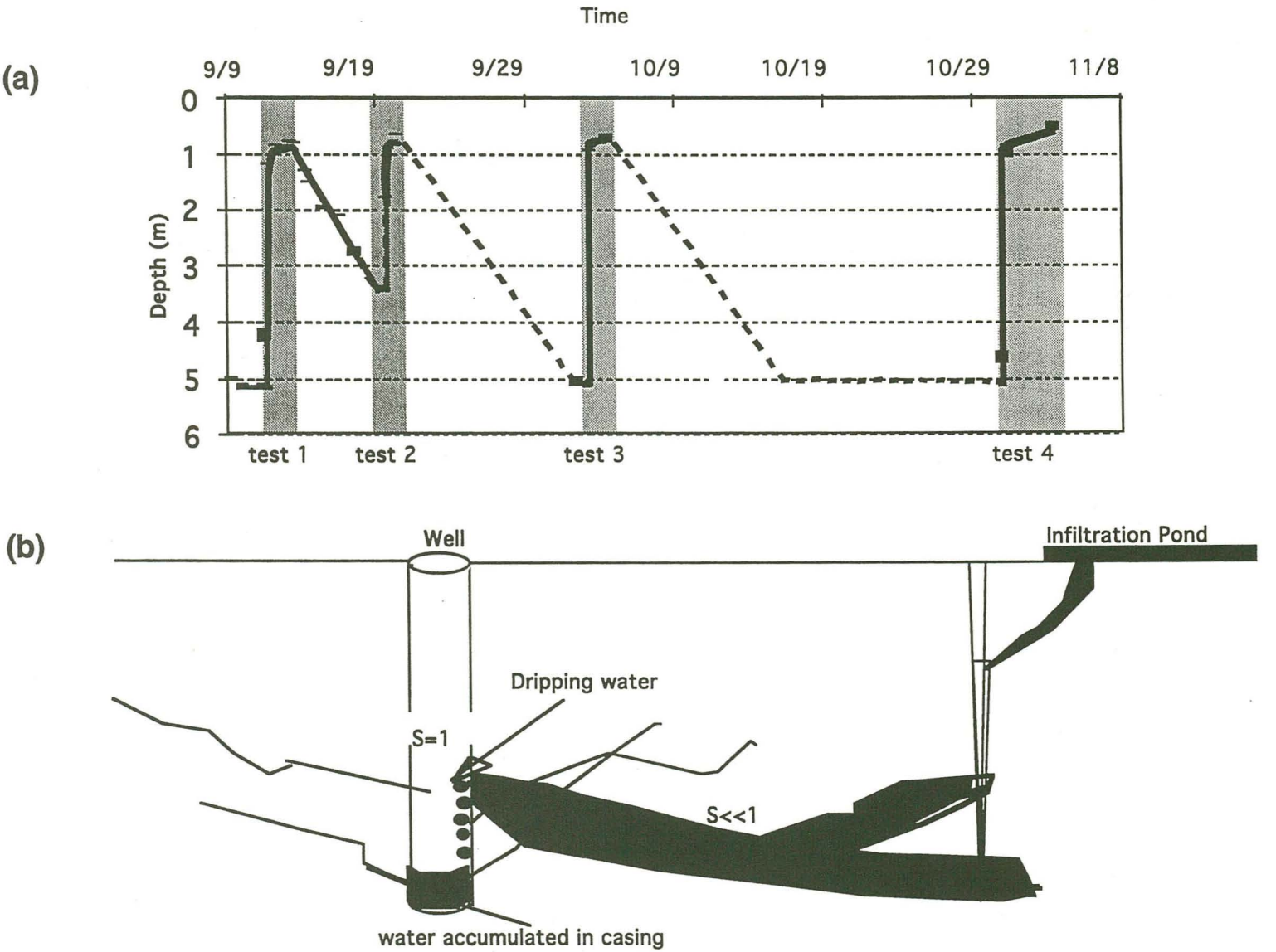

Figure 15. (a) Water level in well I-5 during the 1997 tests. The shaded areas indicate the time during which the surface was ponded; (b) Schematic diagram showing the creation of a water level in an open borehole in fractured rocks.

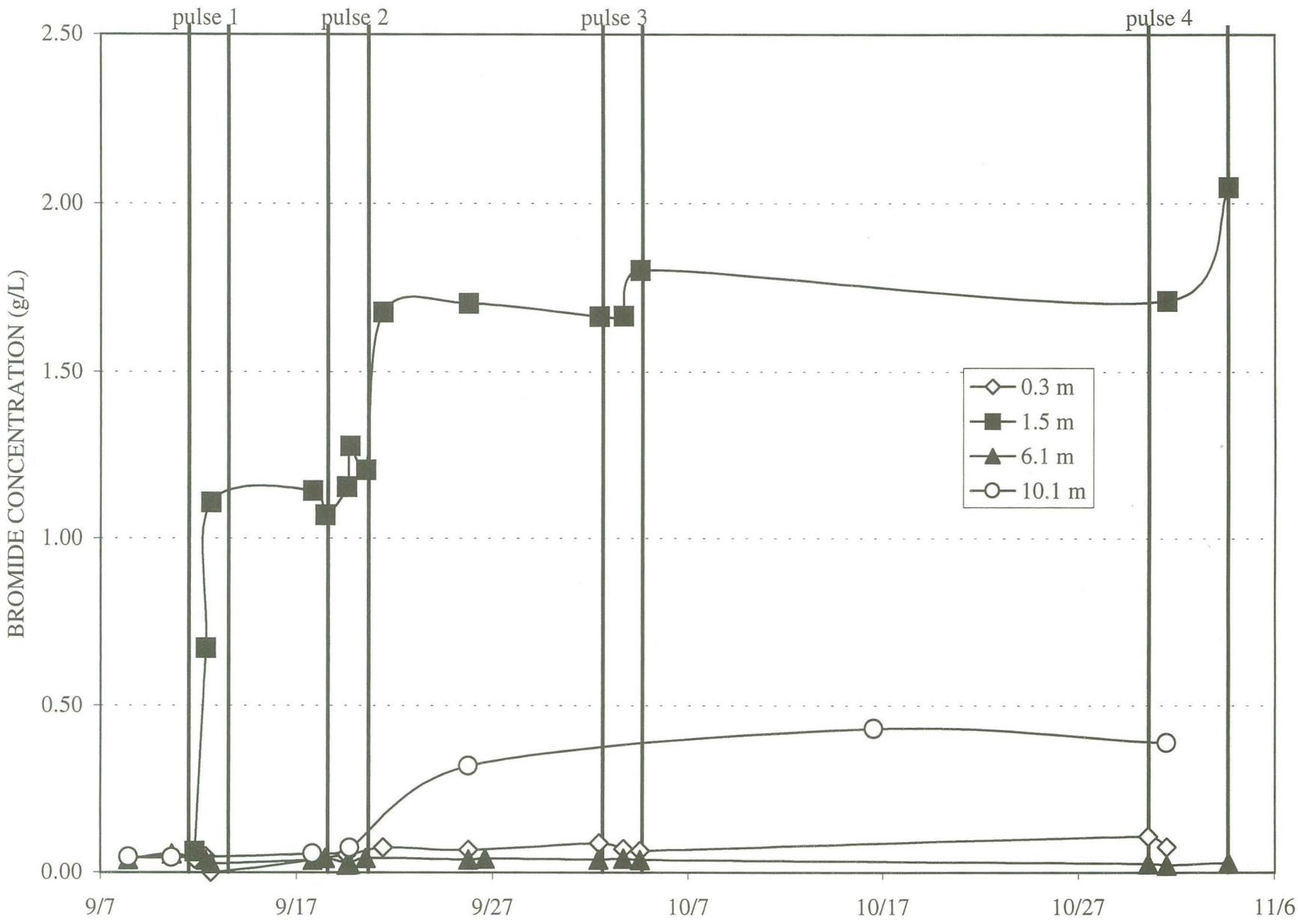

Figure 16. Breakthrough curves for bromide during the 1997 tests for well I-1 at four depths. Note that well I-1 is a vertical borehole within the boundaries of the pond.

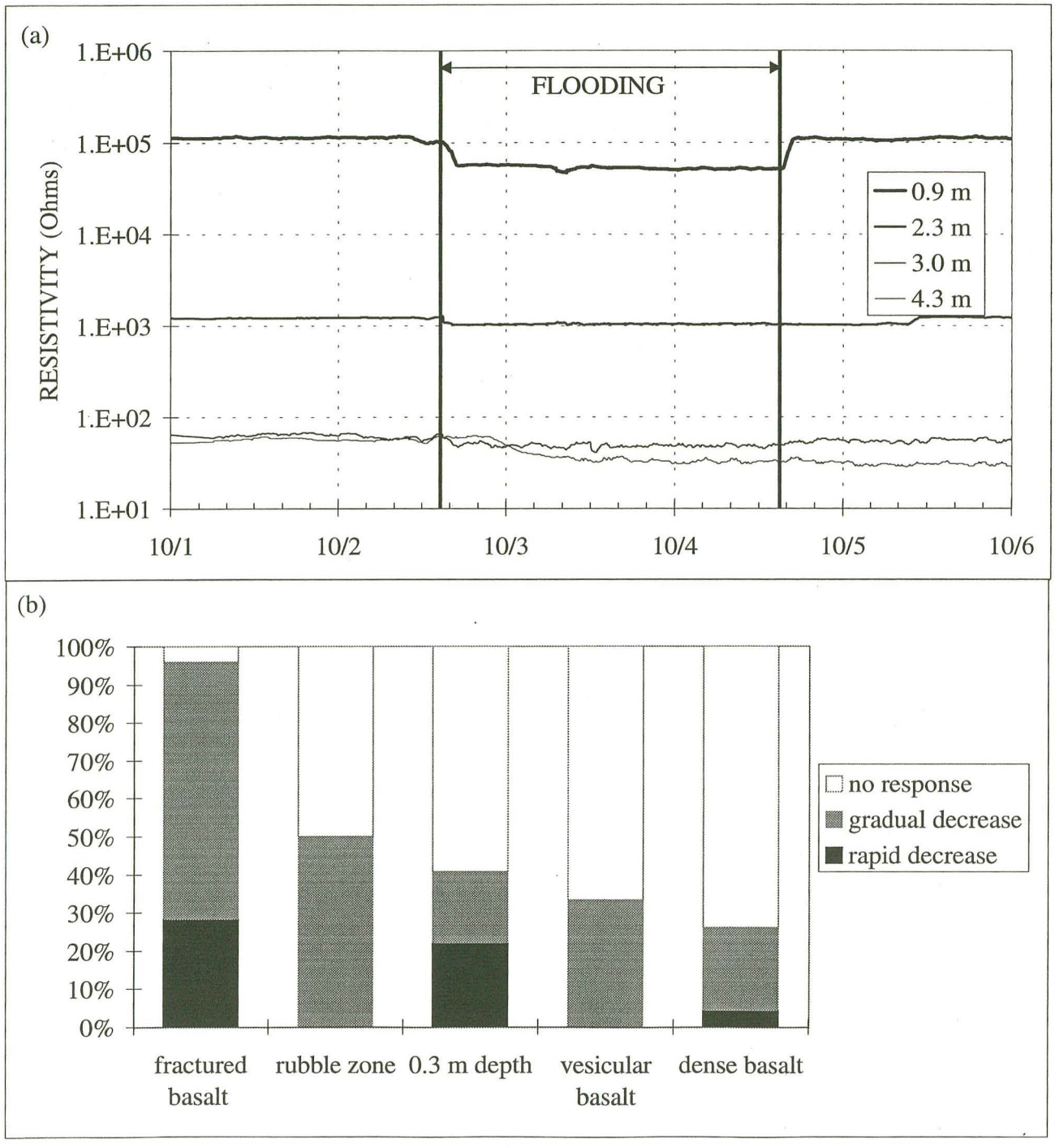

Figure 17. Results of ER probe measurements: (a) example of temporal ER response in well S-2 during test 97-3, and (b) classification of all ER probe measurements during the tests in 1997 given as a percent of ER response types according to lithology.

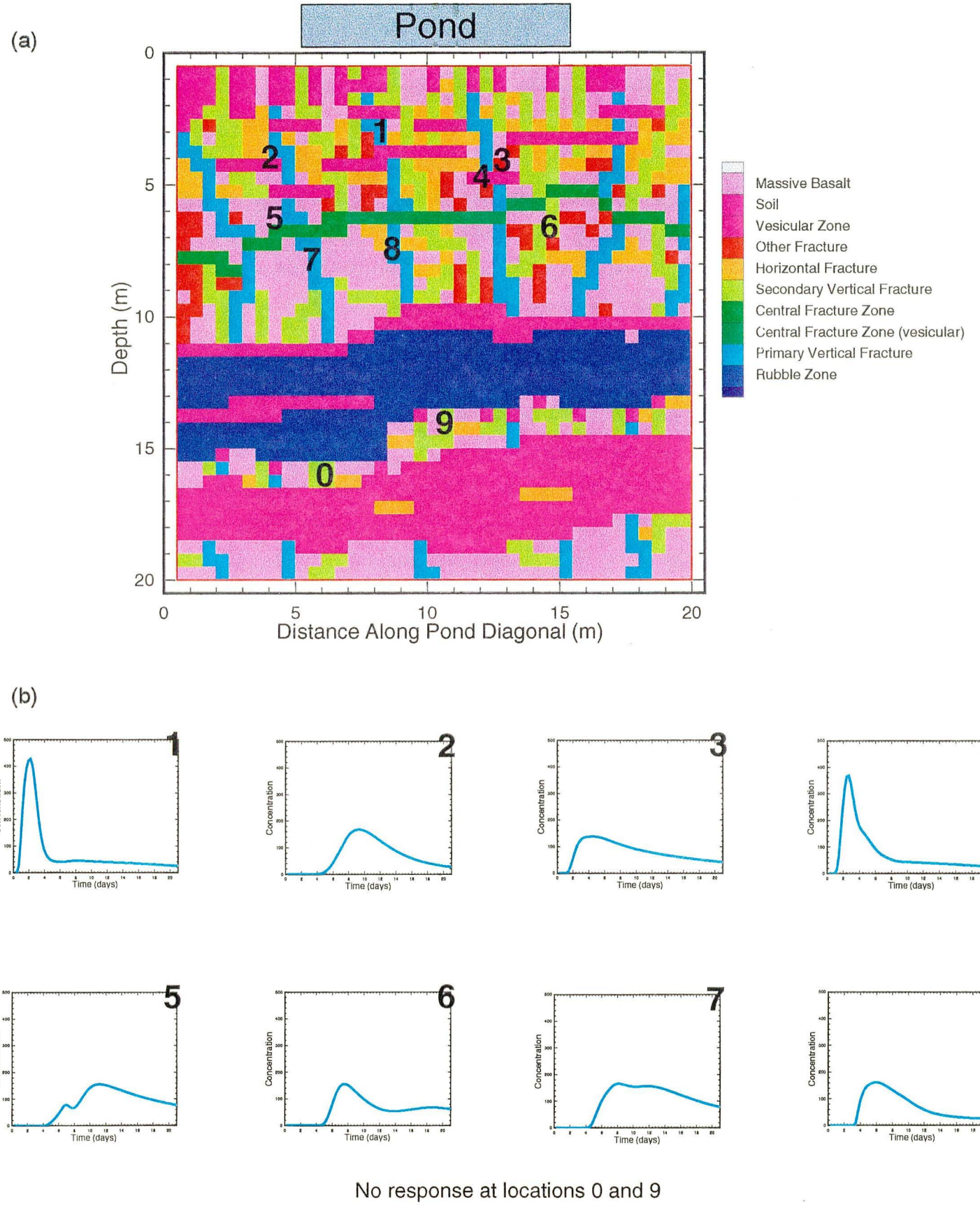

Figure 18. Numerical 2-D modeling of infiltration at the Box Canyon Site: (a) classification of rocks and soils, and (b) breakthrough curves corresponding to numbered locations in (a).

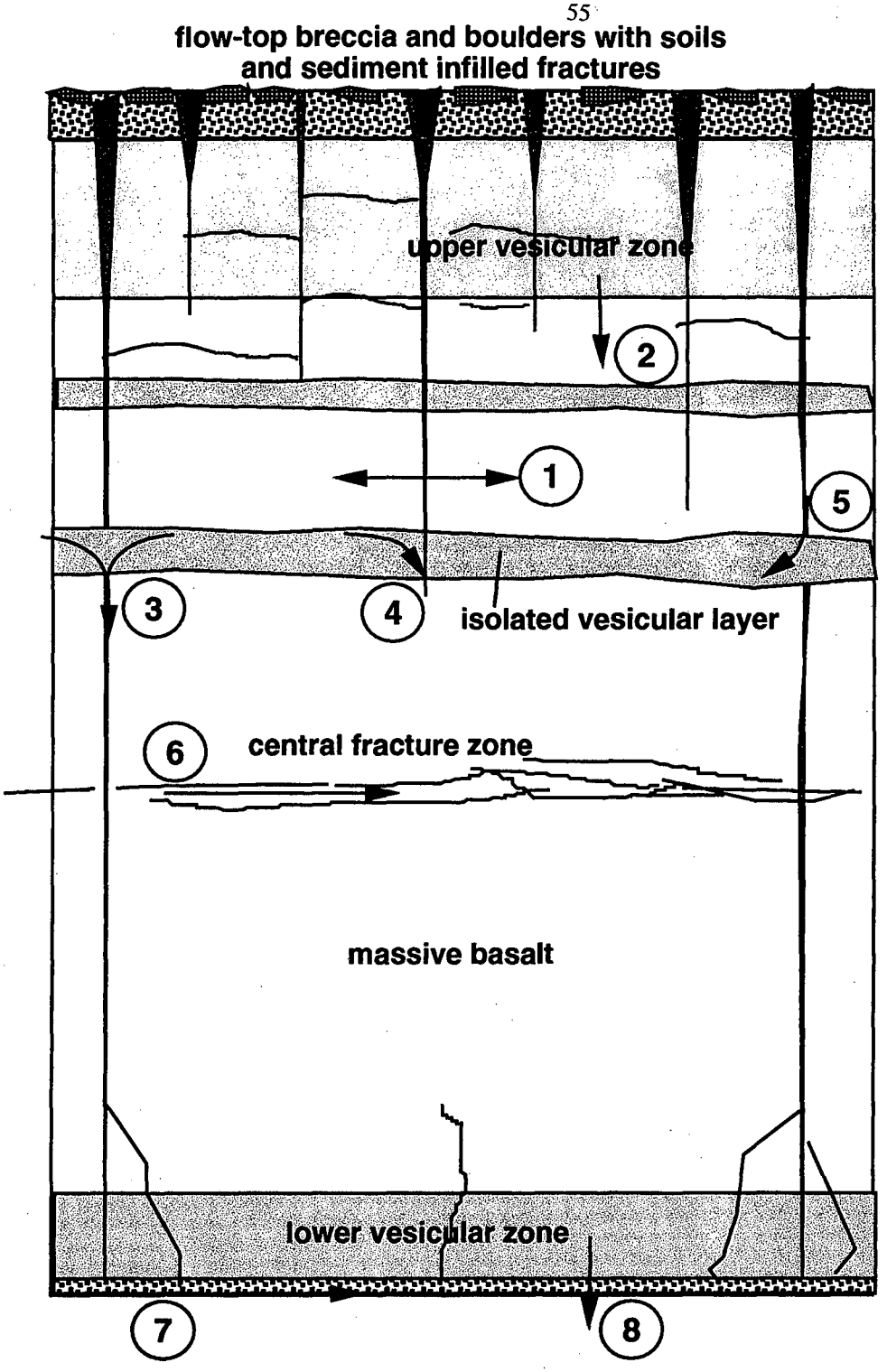

Figure 19. A conceptual model of mechanisms of water flow in a multi-geological-component system representing fractured basalt: (1) fracture-to-matrix diffusion, (2) vesicular basalt-to-massive basalt diffusion, (3) preferential flow through conductive fractures and the effect of funneling, (4) vesicular basalt-to-nonconductive fracture diffusion, (5) conductive fracture-to-vesicular basalt flow and diffusion, (6) lateral flow and advective transport in the central fracture zone, (7) lateral flow and advective transport in the rubble zone, and (8) flow into the underlying basalt flow.

Ernest Orlando Lawrence Berkeley National Laboratory
One Cyclotron Road | Berkeley, California 94720

Prepared for the U.S. Department of Energy under Contract No. DE-AC03-76SF00098